Article

Neuron

Oligodendroglial NMDA Receptors Regulate Glucose Import and Axonal Energy Metabolism

Highlights

- Oligodendroglial NMDA receptors regulate GLUT1 trafficking and glucose import
- Mouse mutants lacking NMDA receptors from oligodendrocytes are delayed in myelination
- Activation of oligodendroglial NMDA receptor supports the axonal energy metabolism
- Mice lacking oligodendroglial NMDA receptors develop late-onset axonopathy and neuroinflammation

Authors

Aiman S. Saab, Iva D. Tzvetavona, Andrea Trevisiol, ..., Johannes Hirrlinger, Frank Kirchhoff, Klaus-Armin Nave

Correspondence

frank.kirchhoff@uks.eu (F.K.), nave@em.mpg.de (K.-A.N.)

In Brief

Saab et al. identify a novel feature of axonal metabolic support. Activation of oligodendroglial NMDA receptors stimulates GLUT1 export and release of lactate. Targeted inactivation of oligodendroglial NMDA receptors in vivo impairs axonal energy metabolism and causes late-onset axonopathy.

Saab et al., 2016, Neuron *91*, 119–132
July 6, 2016
http://dx.doi.org/10.1016/j.neuron.2016.05.016

CellPress

Neuron
Article

Oligodendroglial NMDA Receptors Regulate Glucose Import and Axonal Energy Metabolism

Aiman S. Saab,[1,2,3] Iva D. Tzvetavona,[1] Andrea Trevisiol,[1] Selva Baltan,[4] Payam Dibaj,[1] Kathrin Kusch,[1] Wiebke Möbius,[1,5] Bianka Goetze,[6] Hannah M. Jahn,[1,2] Wenhui Huang,[1,2] Heinz Steffens,[7,8] Eike D. Schomburg,[7] Alberto Pérez-Samartín,[9] Fernando Pérez-Cerdá,[9] Davood Bakhtiari,[5,10] Carlos Matute,[9] Siegrid Löwel,[6] Christian Griesinger,[5,10] Johannes Hirrlinger,[1,11] Frank Kirchhoff,[1,2,5,*] and Klaus-Armin Nave[1,5,*]
[1]Max Planck Institute of Experimental Medicine, Department of Neurogenetics, Göttingen 37075, Germany
[2]Center for Integrative Physiology and Molecular Medicine, Molecular Physiology, University of Saarland, Homburg 66421, Germany
[3]University of Zurich, Institute of Pharmacology and Toxicology, 8057 Zurich, Switzerland
[4]Lerner Research Institute, Cleveland Clinic, Department of Neurosciences, Cleveland, OH 44195, USA
[5]Center Nanoscale Microscopy and Molecular Physiology of the Brain (CNMPB), 37073 Göttingen, Germany
[6]Bernstein Focus for Neurotechnology (BFNT) and School of Biology, Department of Systems Neuroscience, University of Göttingen, 37075 Göttingen, Germany
[7]Institute of Physiology, University of Göttingen, 37073 Göttingen, Germany
[8]Max Planck Institute for Biophysical Chemistry, Department of NanoBiophotonics, 37077 Göttingen, Germany
[9]Universidad del País Vasco, CIBERNED and Departamento de Neurociencias and Achucarro Basque Center for Neuroscience, Leioa 48940, Spain
[10]Department of NMR Based Structural Biology, Max Planck Institute for Biophysical Chemistry, 37077 Göttingen, Germany
[11]Carl-Ludwig-Institute for Physiology, Faculty of Medicine, University of Leipzig, 04103 Leipzig, Germany
*Correspondence: frank.kirchhoff@uks.eu (F.K.), nave@em.mpg.de (K.-A.N.)
http://dx.doi.org/10.1016/j.neuron.2016.05.016

SUMMARY

Oligodendrocytes make myelin and support axons metabolically with lactate. However, it is unknown how glucose utilization and glycolysis are adapted to the different axonal energy demands. Spiking axons release glutamate and oligodendrocytes express NMDA receptors of unknown function. Here we show that the stimulation of oligodendroglial NMDA receptors mobilizes glucose transporter GLUT1, leading to its incorporation into the myelin compartment in vivo. When myelinated optic nerves from conditional NMDA receptor mutants are challenged with transient oxygen-glucose deprivation, they show a reduced functional recovery when returned to oxygen-glucose but are indistinguishable from wild-type when provided with oxygen-lactate. Moreover, the functional integrity of isolated optic nerves, which are electrically silent, is extended by preincubation with NMDA, mimicking axonal activity, and shortened by NMDA receptor blockers. This reveals a novel aspect of neuronal energy metabolism in which activity-dependent glutamate release enhances oligodendroglial glucose uptake and glycolytic support of fast spiking axons.

INTRODUCTION

Oligodendrocytes, best known for making myelin (Emery, 2010; Nave and Werner, 2014), also support the survival of myelinated axons (Griffiths et al., 1998; Kassmann et al., 2007; Lappe-Siefke et al., 2003). Myelin is assembled as a spiral extension of oligodendroglial cell membrane, which requires vesicular transport of membrane material through non-compacted cytosolic channels to the growing tip (Snaidero et al., 2014). In mature myelin, a system of nanometer-wide "myelinic channels" is left behind, the dynamics and dimensions of which were only appreciated with the application of high-pressure freezing (HPF) electron microscopy (Snaidero et al., 2014).

Recently, the identification of metabolic coupling between oligodendrocytes and the axonal compartment, with glycolytic oligodendrocytes providing lactate to axons for aerobic ATP production (Fünfschilling et al., 2012; Lee et al., 2012), has introduced a new paradigm for the interaction of axons and their associated glial cells. However, the concept of glycolytic support by oligodendrocytes (Morrison et al., 2013; Saab et al., 2013) raises the question of how glucose utilization is quantitatively regulated. Since the average spike count rate is the key determinant of axonal ATP consumption, oligodendrocytes need to "know" the spiking activity of myelinated axons, which can differ greatly in vivo (Barry, 2015; Perge et al., 2012). The constitutive overproduction of lactate would result in lactic acidosis, detrimental for white matter function. A plausible preventive mechanism would be that oligodendrocytes "learn" their association with fast spiking axons to adapt their own energy metabolism.

Like unmyelinated axons (Kukley et al., 2007; Wake et al., 2011; Ziskin et al., 2007) also myelinated axons release glutamate upon spiking, which induces calcium elevations in myelin (Micu et al., 2016). Oligodendrocytes could take trace amounts of glutamate as a proxy for axonal spiking activity and energy needs. Indeed, periaxonal spaces underneath myelin are narrow (<50 nm), and glutamate could reach high local concentrations (Stys, 2011).

Oligodendrocytes express different glutamate receptors, including NMDA receptors of unknown function (Káradóttir et al.,

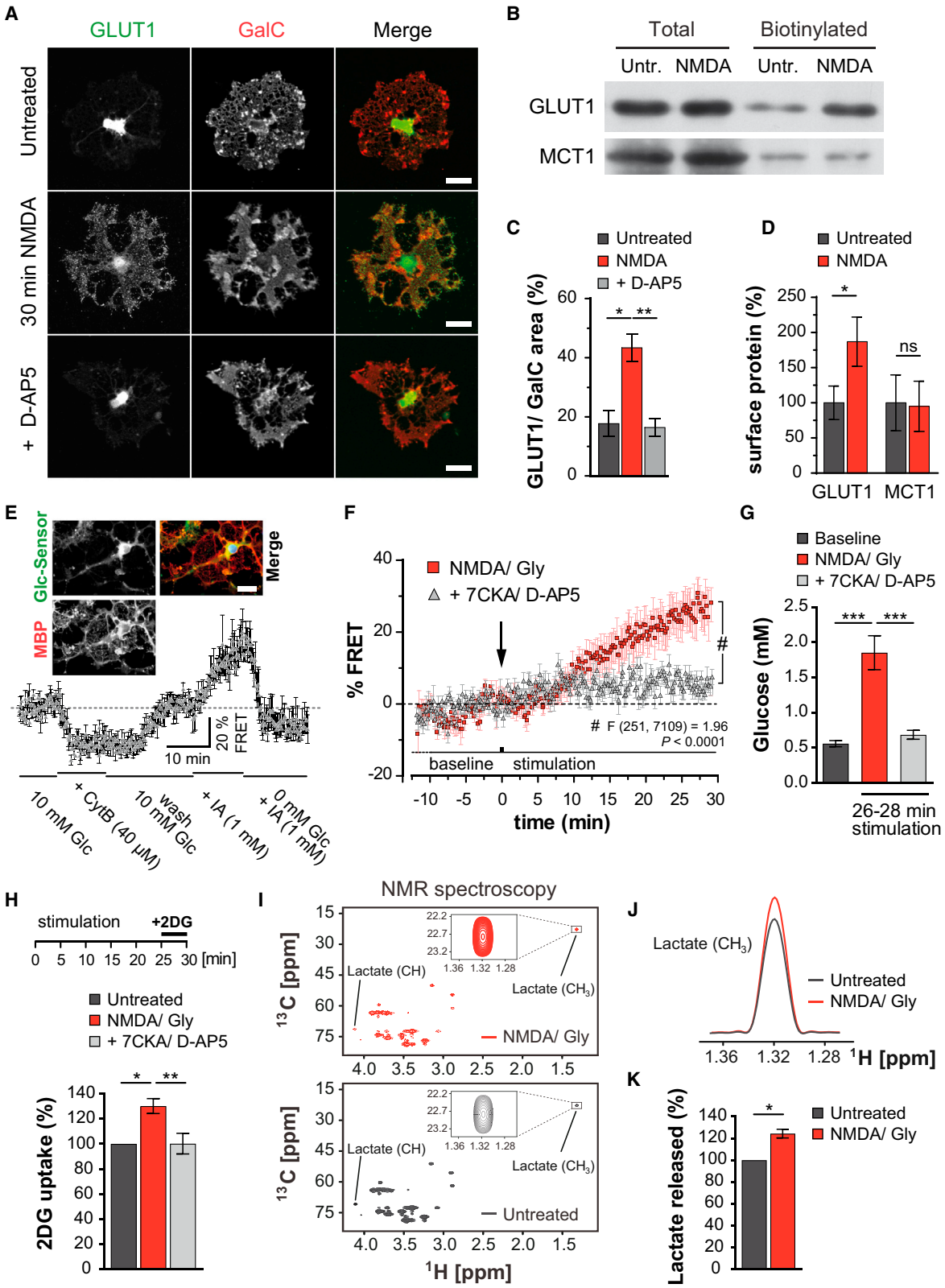

(legend on next page)

2005; Micu et al., 2006; Salter and Fern, 2005). A role for NMDA receptor signaling in oligodendrocyte differentiation and promoting myelination has been suggested, based on in vitro observations (Li et al., 2013; Lundgaard et al., 2013), which is compatible with neuronal activity stimulating OPC proliferation and myelination in vivo (Gibson et al., 2014; Liu et al., 2012). Recently, axonal activity was shown to induce NMDA receptor-mediated calcium increases in myelin, indicating that adult oligodendrocytes have functional NMDA receptors (Micu et al., 2016). However, conditional mouse mutants lacking this receptor from OPC reveal no major abnormality (De Biase et al., 2011; Guo et al., 2012).

NR1 is the obligate subunit of tetrameric NMDA receptors, and expression of its gene (*Grin1*) is higher in OPC than in mature oligodendrocytes (Zhang et al., 2014) but remains detectable throughout adult life (this study). Here, we tested the hypothesis that NMDA receptor signaling to oligodendrocytes is the missing link in coupling axonal activity and ATP consumption to oligodendroglial glucose utilization and lactate supply.

RESULTS

NMDA Receptor Activation Triggers GLUT1 Surface Expression and Enhances Glucose Import in Cultured Oligodendrocytes

Oligodendroglial GLUT1 was localized to intracellular compartments and primary processes (but only weakly to secondary and tertiary processes) and immature myelin membranes (Figure 1A, top). Cultured neurons mobilize glucose transporter GLUT3 in response to glutamate (Ferreira et al., 2011). We therefore asked whether GLUT1, the predominant transporter of oligodendrocytes and astrocytes (Zhang et al., 2014), behaves similarly.

Remarkably, treatment with NMDA triggered GLUT1 redistribution in oligodendrocytes within 30 min, leading to apparent surface expression (Figure 1A, middle) that was efficiently blocked by D-(-)-2-amino-5-phosphonopentanoic acid (D-AP5) (Figures 1A, bottom, and 1C). In contrast, monocarboxylate transporter MCT1 distribution was unaffected by NMDA (Figures S1A and S1B). To confirm that NMDA promotes membrane insertion of GLUT1, we performed biotinylation assays with immunopanned oligodendrocytes (Figure 1B), revealing a 2-fold GLUT1 increase at the cell surface following 30 min NMDA stimulation (Figure 1D), whereas the abundance of MCT1 was the same. To determine functional GLUT1 insertion, we expressed a glucose sensor (Takanaga et al., 2008) in transfected oligodendrocytes (Figure 1E). Activation of NMDA receptors caused a significantly increased FRET signal that was abolished by 7-CKA and D-AP5, which block both the glycinergic and glutamatergic NMDA receptor binding sites, respectively (Figure 1F). Calibration of the FRET sensor allowed the measurement of cytosolic glucose in oligodendrocytes, i.e., 0.56 ± 0.04 mM at baseline and 1.85 ± 0.24 mM following NMDA receptor stimulation (Figure 1G). Finally, we used immunopanned oligodendrocytes and quantified the uptake of 2-deoxyglucose (2DG) to confirm that NMDA elevates glucose import (Figure 1H). In these experiments, elevated glucose was not caused by inhibition of glycolysis because the release of lactate was simultaneously enhanced. By NMR spectroscopy, we calculated a 24% ± 4% increase of U-^{13}C-lactate release originating from U-$^{13}C_6$-labeled glucose (Figures 1I–1K). As expected, lactate release from cultured oligodendrocytes relies on glucose availability (Figures S1C and S1D). However, NMDA-stimulated lactate release was unexpected (Figures 1I–1K and S1E) because basic metabolic demands did not change, and there were no signs of oligodendrocyte death (Figure S1F). Most likely, membrane repolarization (triggered by NMDA receptor signaling and ion influx) consumes the additional ATP and leads to more glycolysis with lactate release.

Myelination In Vivo in the Absence of Oligodendroglial NMDA Receptors

Glucose is a major carbon source for lipid precursor metabolites, which are rate-limiting for myelination (Rinholm et al., 2011).

Figure 1. NMDA Stimulates GLUT1 Surface Expression and Glucose Uptake by Cultured Oligodendrocytes

(A) Oligodendrocyte immunostained for GLUT1 and GalC. NMDA receptor stimulation mobilizes GLUT1 and increases its cell surface expression, which is blocked by D-AP5. Scale bar, 20 μm.

(B) GLUT1 and MCT1 immunoblots following cell surface biotinylation of immunopanned NMDA-treated oligodendrocytes and controls.

(C) Quantification of the experiments giving the ratio of GLUT1:GalC in a stained area of n = 3 experiments and 20–24 cells per condition (*$p < 0.05$, **$p < 0.01$ one-way ANOVA with Bonferroni's multiple comparisons test).

(D) Quantification of the experiments in (B), normalizing biotinylated to total protein ($p = 0.03$, n = 3; paired t test). MCT1 surface expression is unchanged.

(E) FRET imaging of oligodendrocytes expressing a glucose sensor (Takanaga et al., 2008) (FLII12Pglu-700μΔ6). Intracellular glucose levels (normalized to baseline FRET signals, n = 4) drop with addition of cytochalasin B (CytB, glucose transporter blocker) or increase with iodoacetate (IA, glycolysis inhibitor). Note that intracellular glucose is rapidly phosphorylated and undetectable.

Inset: oligodendrocyte transfected with the glucose sensor and counterstained for MBP. Note that the sensor is mainly located in the soma and main processes. Scale bar, 20 μm.

(F) NMDA receptor stimulation (by applying 100 μM NMDA and glycine) increases FRET signals that can be blocked by the addition of 7CKA and D-AP5 ($F_{interaction}(251, 7{,}109) = 1.96$, $p < 0.0001$, two-way ANOVA).

(G) Quantification of calibrated FRET signals of NMDA-stimulated oligodendrocytes (26–28 min), compared to baseline and cells also receiving 7CKA and D-AP5 (***$p < 0.001$, one way ANOVA with Bonferroni's multiple comparisons test).

(H) Immunopanned oligodendrocytes stimulated with NMDA/Gly (25 min) before switching to 2-deoxyglucose (2DG, 10 mM, 5 min). Increased 2DG uptake was blocked by 7CKA and D-AP5 (n = 5 experiments, *$p < 0.05$, **$p < 0.01$; paired t test).

(I) ^{13}C, ^{1}H-HSQC spectra at 700 MHz corresponding to proton resonance from the culture medium of immunopanned oligodendrocytes 30 min after exposure to NMDA/Gly (top) and controls (bottom). Boxed: lactate signals. Quantification by comparison of the peak volume of lactate methyl group to the internal standard DSS.

(J) Increased lactate following NMDA/Gly treatment, depicted by overlaying the 1D-^{1}H slices of spectra in the lactate methyl signal range.

(K) Lactate release after NMDA receptor stimulation increased to 124% ± 4% (n = 4 paired NMR experiments, $p = 0.023$ paired t test).

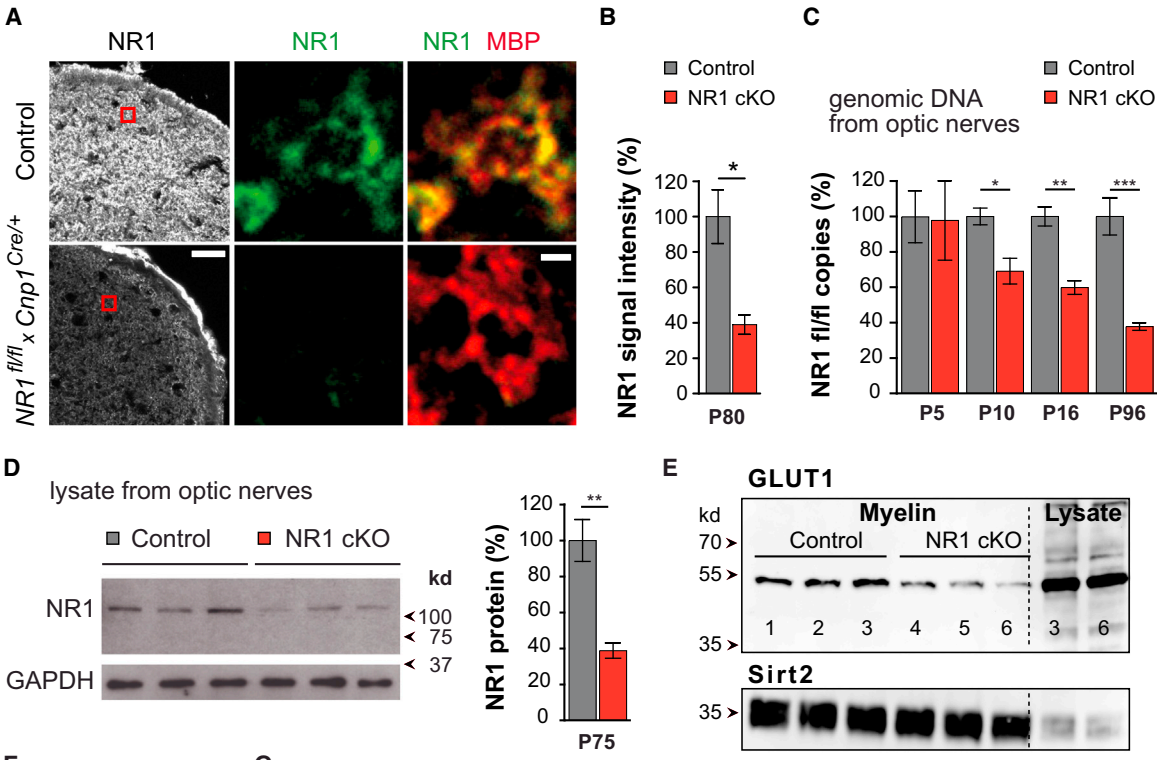

(legend on next page)

In vivo, reduced glutamate signaling might thus affect myelination during development. To study oligodendroglial NMDA receptor function, we crossed mice with a floxed *NR1* allele (Tsien et al., 1996) to $Cnp1^{Cre/+}$ mice (Lappe-Siefke et al., 2003). NR1 (gene symbol *Grin1*) encodes the obligatory subunit of functional NMDA receptors (Tsien et al., 1996).

In $Grin1^{flox/flox}$*$Cnp1^{Cre/+}$ mice (hereafter termed NR1 mutant or cKO, with $Grin1^{flox/flox}$*$Cnp1^{+/+}$ and $Grin1^{flox/+}$*$Cnp1^{Cre/+}$ being controls), NR1 was lost by immunostaining, as shown for optic nerve (Figures 2A, 2B, and S2A), by qPCR of genomic DNA and by western blot analysis (Figures 2C and 2D). Recombination analysis revealed that at P5, when the optic nerve is already populated with oligodendroglial precursor cells (OPCs), loss of the floxed allele was not yet significant. However, at P10, when many oligodendrocytes had matured and express Cnp1, about one-third of the floxed alleles were excised, and recombination reached 62% ± 8% at P96, when myelination is completed, matching the expected proportion of oligodendrocyte in adult optic nerves (Miller et al., 1985). Cre-mediated reporter expression in optic nerves demonstrated that virtually all recombined cells were of oligodendroglial origin (Figures S2B and S2C). NR1 expression in astrocytes and OPCs could account for the remaining 40% NR1 signal of whole optic nerve immunostainings (Figure 2B) or protein lysates (Figure 2D).

In purified myelin from mutant brains, we found a strong reduction of GLUT1 (but not MCT1) compared to controls (Figures 2E, 2F, S1G, and S1H), whereas total tissue GLUT1 was unchanged in NR1 mutants. By immunogold labeling of mature optic nerves, GLUT1 was localized in the myelin sheath, in the outer tongue, and in the paranodal loops (Figure 2G), well positioned for functional glucose uptake into the system of myelinic channels.

GLUT1 abundance in myelin sheaths of optic nerve axons was reduced by 80% in NR1 mutants compared to littermate controls (Figures 2H), in line with its NR1-dependent mobilization in cultured oligodendrocytes.

GLUT1 mRNA is more abundant in mature oligodendrocytes than in precursor cells (Zhang et al., 2014). From CNS white matter samples, we amplified equal amounts of GLUT1 and MCT1 cDNA when comparing mutants and controls, indicating that NMDA receptor signaling does not regulate GLUT1 at the level of gene expression (Figure S1I). Interestingly, we localized MCT1 by immuno-electron microscopy at both the outer and inner tongue of myelin (Figure 2I). Thus, lactate transporters are strategically positioned for taking up and supplying glycolysis products (Fünfschilling et al., 2012; Lee et al., 2012).

Phenotypically, mutant mice were normally developed with functional white matter tracts, as shown for the optic nerve (Figure S3), and are long-lived. This suggests that NMDA receptors are not essential for myelination per se, in agreement with earlier reports (De Biase et al., 2011; Guo et al., 2012). However, the paucity of GLUT1 in myelin (Figures 2E, 2F, and 2H) suggested reduced glucose import, which could affect the rate of myelin growth that is metabolically controlled (Rinholm et al., 2011). In the rodent optic nerve, the highest myelination rate occurs during the third postnatal week (Hildebrand and Waxman, 1984) and predicts the highest demands for glucose as a carbon source for lipid synthesis at this time. Indeed, by EM we noted at ages P18–P20 that myelin was thinner, with fewer myelinated axons in the mutant optic nerves (Figures 3B and 3D–3G). This difference was only transient as adult (P70) NR1 mutant optic nerves "catch up" and exhibit a normal myelin sheath thickness (Figures 3C, 3H, and 3I).

Functional Analysis of Myelinated Axons

To study function, we assessed optic nerve conduction at different stages of development by recording compound action potentials (CAPs) ex vivo, comparing NR1 mutant and controls (Figure S4). CAP profiles revealed a transiently reduced conduction velocity, again only at the peak of myelination (age P19–P21) and mainly affecting small caliber axons (Figures S4D–S4F). These are best explained by the delay of CNS myelination (Figures 3D–3I), as nerve caliber and axon numbers were normal (Figures S4J and S4K). The developmental delay of myelination in NR1 mutant optic nerves fits well the unexplained observation that demyelinating lesions repair less well when NMDA receptors are blocked (Li et al., 2013; Lundgaard et al., 2013).

Next, we examined myelinated optic nerves under metabolic stress for their ability to recover from transient oxygen-glucose deprivation (OGD), a well-established model of acute ischemia (Tekkök et al., 2007). Optic nerves were acutely isolated

Figure 2. Oligodendroglial NMDA Receptor Mutants with Reduced GLUT1 Incorporation into Myelin

(A) Immunostaining of NR1 in optic nerve cross sections at age P80 from control and NR1 cKO mice (left panel). Higher magnifications (middle and right panels) reveal that NR1 (green) is absent from mutants and overlaps with MBP (red) in control mice. Scale bars, 20 μm (left) and 1 μm. See also Figure S2A.

(B) Quantitation of NR1 staining intensity from whole optic nerve sections (n = 3; p = 0.019, Student's t test).

(C) Cre-mediated recombination of genomic DNA in individual optic nerves of each genotype as quantified by qPCR. Depicted is the relative abundance of the floxed NR1 allele after recombination (normalized to the abundance in $NR1^{fl/fl}$ littermate controls, defined as 100% at different ages). In NR1 mutant nerves, the abundance of NR1 flox copies was determined at ages P5 (98% ± 22% flox copies remaining; n = 5 versus 4, p = 0.939), age P10 (69% ± 7%; n = 4, p = 0.0119), age P16 (60% ± 4%; n = 4 versus 3, p = 0.0024), and P96 (38% ± 2%; n = 4 versus 9, p < 0.0001).

(D) Western blot analysis of NR1 expression in individual nerves from mutant and control mice at age P75. Quantification revealed a reduction by 61% ± 12% in NR1 cKO nerves (n = 3, p = 0.0079). GAPDH, loading control.

(E) By western blotting, GLUT1 is reduced in purified myelin of NR1 mutants (Sirt2, loading control).

(F) Quantification of E (n = 3; p = 0.008, Student's t test).

(G) Localization of GLUT1 by immunogold labeling. In optic nerve cross sections, GLUT1 was detected in myelin sheaths, the outer tongue, and paranodal loops. Scale bar, 200 nm. Gold particles, red arrows.

(H) Reduced abundance of immunogold labeled GLUT1 in myelin of NR1 mutant optic nerves when compared to littermate controls (10–12 randomly taken images per animal, n = 3; p = 0.0025, Student's t test).

(I) By immunogold labeling, MCT1 is associated with adaxonal (outer tongue) and abaxonal (inner tongue) myelinic channels, without difference between mutants and controls. Scale bar, 100 nm.

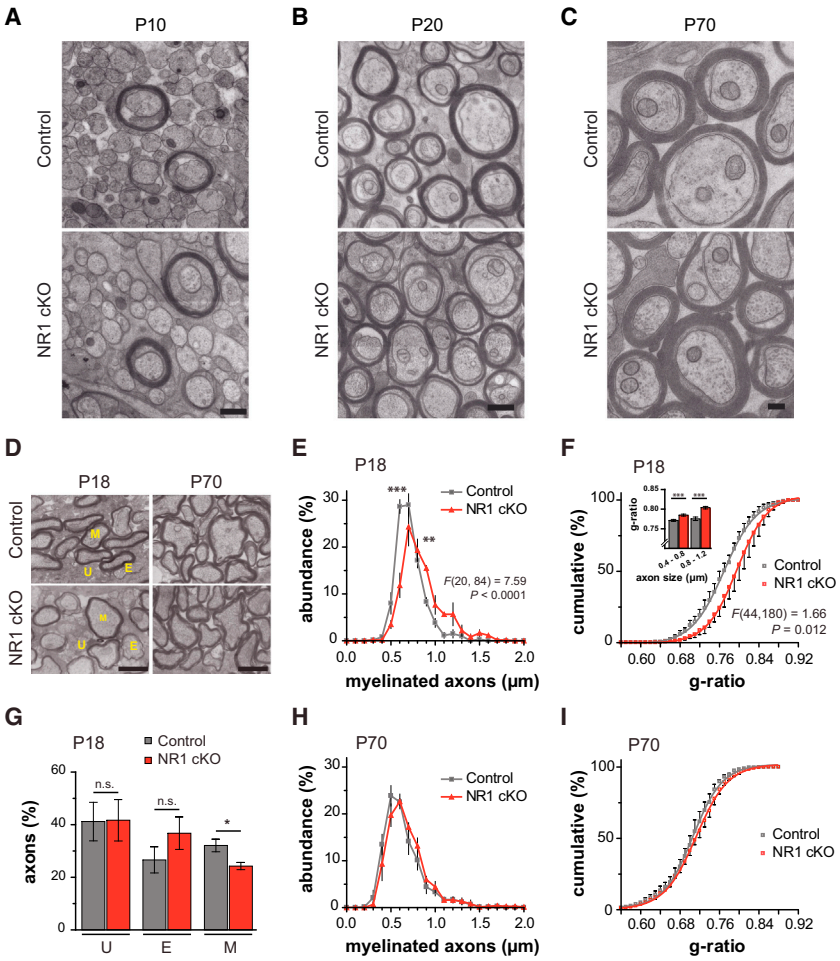

Figure 3. Myelination in the Absence of Oligodendroglial NMDA Receptors In Vivo

(A–C) High-pressure freezing (HPF) electron microscopy of the developing optic nerve.

Overview of optic nerve cross sections from control and NR1 mutant mice at P10 (A), P20 (B), and P70 (C). At early and late stages, NR1 mutant nerves are indistinguishable from controls. A minor hypomyelination is apparent at P20. Scale bars, 0.5 µm (A and B) and 0.2 µm (C).

(D) Electron microscopy of conventionally fixed optic nerves from mutant and controls, with unmyelinated (U), ensheathed (E), and myelinated (M) axons. Scale bar, 1 µm.

(E–I) Axon size distribution and myelin sheath thickness (g-ratio) at P18 and P70.

(E) Diameter spectrum of myelinated axons with relatively more myelinated small caliber axons in control nerves than in NR1 cKO at P18 (***$p < 0.001$, two-way ANOVA, Bonferroni's post-test).

(F) Cumulative frequency of g-ratios (low to high) measured for individual optic nerves of each genotype. Note the significant shift to higher g-ratios in P18 NR1 mutants (inset: means ± SEM of all g-ratios for two axon size groups).

(G) At P18, myelinated (M) axons are transiently reduced in mutant optic nerves, unlike the number of unmyelinated (U) and merely ensheathed (E) axons (400–700 axons counted per nerve; n = 3, p = 0.048).

(H and I) Axon size distribution (H) and optic nerve g-ratios (I) are similar in mutants and controls.

Causality of NMDA Receptor Signaling and Glucose Metabolism in Axonal Support

To demonstrate causality between oligodendroglial glucose metabolism and axonal recovery, we asked whether lactate, permeating through MCT1 (Figures 2I), can replace glucose as an energy source and restore conduction independent of prior NMDA receptor signaling. As predicted, using lactate-containing ACSF for reperfusion, optic nerves from NR1 mutants recovered as well as control nerves and even better than in the presence of glucose (Figures 4D and 4E). This confirms that axons readily use lactate for ATP generation (Fünfschilling et al., 2012; Lee et al., 2012; Tekkök et al., 2005; Wyss et al., 2011). More importantly, it also proves that optic nerves in NR1 mutants are not per se more susceptible to axonal injury. We confirmed this experimentally with MOG-induced experimental allergic encephalomyelitis (EAE), associated with secondary axonal dysfunction. Here, we found no difference in the onset of EAE symptoms or in clinical severity (Figures S5B–S5D), as indicated earlier (Guo et al., 2012; Matute, 2010).

During OGD, abnormal Ca^{2+} entry into the axonal compartment triggers axon loss probably resulting from excessive glutamate signaling caused by reversal of glutamate transporters (Stirling and Stys, 2010; Tekkök et al., 2007). Indeed, in the absence of free extracellular Ca^{2+}, the axonal recovery was almost 100% in control nerves yet remained significantly impaired in NR1 mutants (Figures S6E and S6F). Thus, glucose

and CAPs were recorded ex vivo (Figure 4A, top). In these experiments, all optic nerves maintained conductivity (defined as "CAP area" of 1.0) and, within minutes after OGD onset, displayed block of nerve conduction, as illustrated by the rapid decline of CAP area (Figures 4A and 4B). When re-perfused 60 min later using oxygenated artificial cerebrospinal fluid (ACSF, 10 mM glucose), we determined some persistent loss of conduction in wild-type nerves, a Ca^{2+}-dependent damage to axons (Tekkök et al., 2007). Surprisingly, in NR1 mutant nerves the recovery of axon function was further reduced by 50% (Figures 4C). NMDA-receptor-mediated excitotoxicity in oligodendrocytes (Káradóttir et al., 2005; Micu et al., 2006; Salter and Fern, 2005) may not be the main mechanism causing myelin damage (Hamilton et al., 2016). Indeed, ultrastructural damage following OGD alone, such as myelin delamination, was the same in NR1 mutants and controls (Figure S5A). Thus, further loss of axonal conductivity was not caused by more severe myelin injury, but rather by less-efficient axonal recovery from the metabolic stress of OGD. Importantly, axonal recovery after OGD was normal prior to age P10 (Figure S6A), suggesting that axons require oligodendroglial support mostly after myelination, which limits rapid axonal access to extracellular metabolites (Nave, 2010).

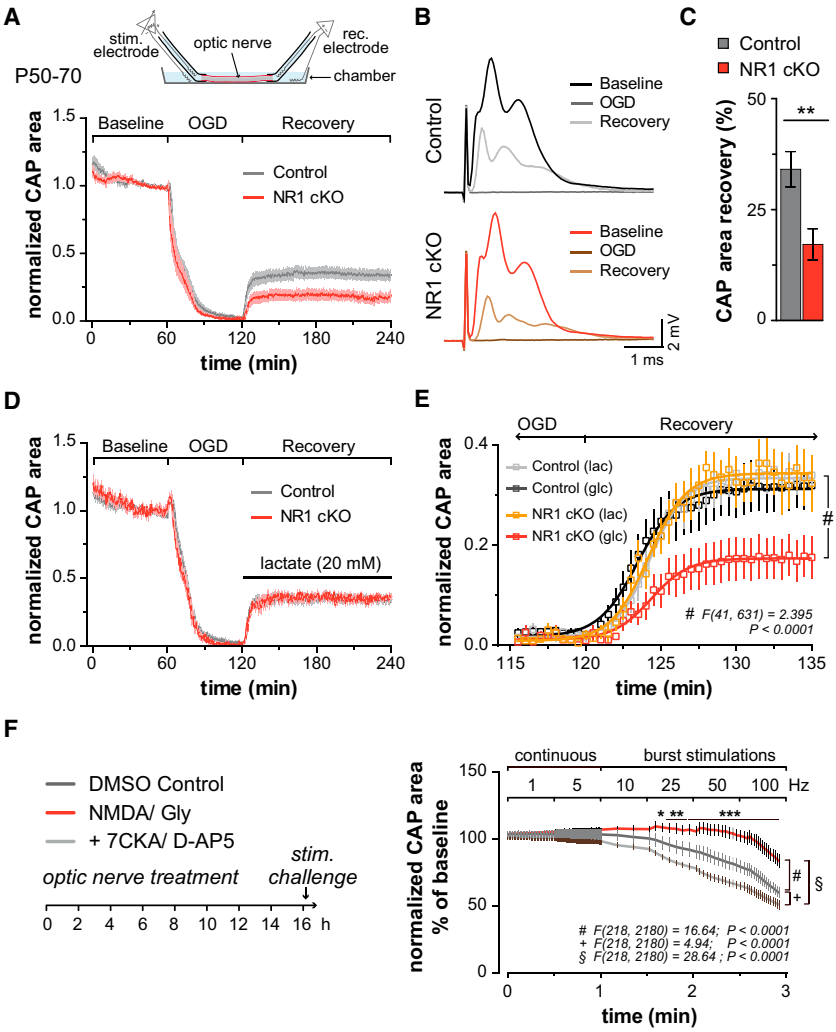

Figure 4. Axonal Energy Metabolism Regulated by NMDA Receptor and GLUT1-Dependent Lactate Export from Myelinating Oligodendrocytes

(A) Top: scheme of recording compound action potentials (CAPs) from acutely isolated optic nerves. After 1 hr, nerves were subjected to 60 min oxygen glucose deprivation (OGD) followed by reperfusion with ACSF containing 10 mM glucose. Bottom: optic nerve CAP areas (i.e., area underneath CAPs as shown in C) normalized to baseline. Note the rapid decline of nerve conduction and the incomplete recovery after reperfusion, which is more pronounced in NR1 mutants (red) compared to controls (black).

(B) Averaged optic nerve CAPs during baseline, OGD, and recovery phase in control (top) and NR1 cKO (bottom).

(C) Quantification of data in (A) with reduced functional recovery after OGD in mutants (n = 12) versus controls (n = 11, p = 0.0046, Student's t test).

(D) With 20 mM lactate, the functional recovery after OGD was the same in NR1 mutants (n = 6) and controls (n = 8).

(E) Axonal recovery at higher temporal resolution, comparing 10 mM glucose (glc) and 20 mM lactate (lac). Depicted are fitting curves (lines, Boltzmann fit) for the average CAP area over time ($p < 0.0001$, two-way ANOVA comparing glucose and lactate in NR1 mutants).

(F) Wild-type optic nerves, maintained functional ex vivo for 16 hr in the presence of NMDA/Gly (100 μM), or NMDA/Gly plus 7CKA/D-AP5 (100 μM), or only DMSO (control), were subsequently challenged with increasing stimulation frequencies. Note that nerves treated with NMDA/Gly show less decline of CAP area at higher frequency ($p < 0.0001$ two-way ANOVA with Dunnett's multiple comparisons test, n = 6 nerves for each treatment group).

uptake by oligodendrocytes is critical to reenergize axons independent of Ca^{2+}-mediated damage.

We suggest that NMDA receptor signaling to oligodendrocytes enhances incorporation of GLUT1 into oligodendroglial and myelin membranes (providing "hardware" of glycolytic support), specifically around axons of higher electrical activity. Interestingly, when optic nerves were acutely isolated from wild-type mice and tested an hour later, the prior application of D-AP5, 7CKA, or MK801 (30 min before the onset of OGD) did not visibly reduce axonal recovery from OGD (Figure S6F), in line with older reports (Tekkök et al., 2007). This is no contradiction to the mutant phenotype in vivo, however, because development and pharmacology operate at different timescales, and it could take hours or days to lose functionally exposed GLUT1 from the myelin compartment. Indeed, wild-type optic nerves maintained for an extended time ex vivo, and then tested for conductivity, revealed an intriguing effect of both NMDA and NMDA receptor blockers. In the presence of glucose and oxygen, their basic conduction properties appeared unchanged after 16 hr (Figure S6G). We then studied axon function under metabolic challenge but chose a more physiological and graded paradigm than OGD. Optic nerves were stimulated by short bursts with a gradual increase in frequency (between 1 and 100 Hz). As expected, the recorded CAPs declined as a function of increasing frequency (Figures 4F). Interestingly, when nerves were preincubated for 16 hr in the presence of 100 μM NMDA/Gly (mimicking glutamate release from spiking axons), high-frequency conductivity was much better maintained (Figure 4F). For example, NMDA-stimulated nerves appeared well able to maintain axonal conduction at 25 Hz, but without prior NMDA exposure axons stimulated at 25 Hz showed a functional decline of about 10% per min. Consistently, the decline of axonal conduction at increasing frequency of stimulation was even more aggravated when NMDA receptors had been blocked before by D-AP5 and 7CKA (Figure 4F). Taken together, these results strongly suggest that non-spiking axons lose oligodendroglial metabolic support over time.

In Vivo Relevance of Oligodendroglial NMDA Receptor Function

To confirm our key finding also in vivo, we focused on the spinal cord. Electrical stimulation of dorsal roots (L4) in anesthetized

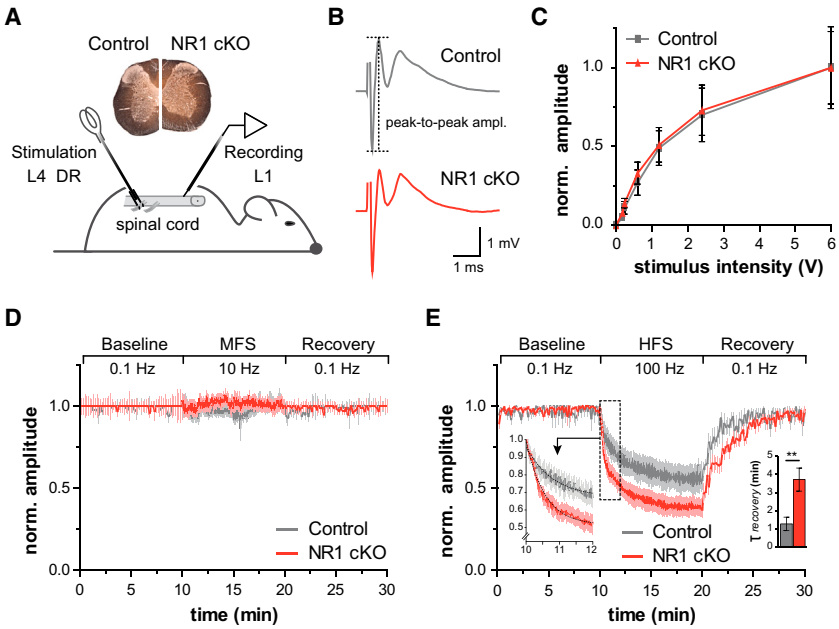

Figure 5. Requirement of Oligodendroglial NMDA Receptors for High-Frequency Conduction

(A) Scheme of stimulating DRG axons of lumbar segment L4 and recording from fasciculus gracilis at L1 (inset: intact myelination of spinal cord in mutants and controls, Gallya's stain).

(B) Representative CAPs (averaged) in control (top) and mutants at age 4–6 months. Dotted line: peak-to-peak amplitude used to analyze firing strength of fastest axon groups. Conduction delays were unchanged.

(C) Normal axonal excitability in mutants measured at increasing stimulus intensities with peak-to-peak amplitude normalized to maximal readings.

(D) After 10 min at 0.1 Hz, stimulation frequency increased to 10 Hz (medium frequency stimulation, MFS), showing no difference between mutants (n = 6) and controls (n = 3).

(E) 100 Hz (high frequency stimulation, HFS) caused a decrease of firing strength (within seconds) that was significantly faster and stronger in NR1 mutants (n = 7) than controls (n = 5). Left inset: higher temporal resolution for indicated region, $F_{interaction}$ (119, 1,190) = 3.07, $p < 0.0001$, two-way ANOVA). Right inset: slower recovery of CAPs at the end of HFS, monitored at 0.1 Hz (τ calculated from normalized exponential fits, $p = 0.0084$, Student's t test).

mice evoked stable CAPs that could be recorded from the dorsal columns (L1) (Figure 5A). We detected no overt differences between NR1 mutants and controls in spinal conduction properties or axon excitability (Figures 5B and 5C), confirming the overall integrity of myelinated tracts (Figures 5A, inset). Next, we monitored CAP (peak-to-peak) amplitudes following challenges at low (0.1 Hz), medium (10 Hz) and high frequency (100 Hz). At low or medium frequency (for 10 min), we observed no difference between mutants and controls (Figures 5D). However, upon high-frequency stimulation, CAP amplitudes dropped significantly faster in mutant mice (Figures 5E, inset left). When allowed to recover at low frequency (0.1 Hz), CAPs in mutant spinal cords recovered more slowly than in controls (Figures 5E, inset right).

Myelinated axons vary in length, diameter, and firing frequencies, suggesting that their long-term energy demands differ greatly (Perge et al., 2012). We anticipated that NR1 mutant mice with a developmentally reduced presence of GLUT1 in myelin sheaths develop at least some signs of axonal pathology. We therefore examined white matter integrity in different CNS regions of adult NR1 mutants and controls, kept under normal cage conditions (10–12 months) and without specific challenges. While most white and gray matter regions in mutant mice, including optic nerves, appeared devoid of pathology within the first year (data not shown), such changes became detectable in white matter tracts of the medulla (Figures 6A and S7A). In longitudinal sections, we observed an increased abundance of reactive microglia and astrogliosis (Figures 6A–6D). Also in spinal cord cross sections we occasionally noticed reactive microglia in white matter tracts of the dorsal and lateral columns (Figures S7B and S7C). By electron microscopy, we observed myelin delamination and degenerating axons in cervical spinal cord sections (Figures 6E and 6F) that were not a feature of wild-type mice.

The majority of myelinated axons in cortico-spinal tracts fire at a high frequency and comprise a high energy demanding white matter tract (Perge et al., 2012). We therefore performed a motor-behavioral analysis to assess the function of spinal tracts in adult NR1 mutant mice. Indeed, even on a simple rotarod test, 1 year old NR1 mutants revealed a significant deficit in performance when compared to age-matched controls (Figure 6G).

At the age of 19 months, NR1 mutants exhibited a severe neurological phenotype including hind limb clasping, hunchback, and ataxia (Figure 6H) caused by ongoing neurodegeneration, which became visible at 10 months. Signs of neuroinflammation and axonopathy were seen in all CNS white matter tracts (Figures 6I–6L).

DISCUSSION

Oligodendroglial metabolic support can explain why myelinated axons are vitally dependent on myelin integrity, independent of the myelin function in saltatory conduction (Griffiths et al., 1998; Kassmann et al., 2007; Lappe-Siefke et al., 2003). However, the question arises as to how glycolysis in oligodendrocytes is matched to different axonal energy needs and how excessive lactate production is avoided. Our study yields a novel working model in which oligodendrocytes regulate glucose utilization by using NMDA receptor signals as a surrogate marker for axonal spiking activity (Figure 7).

While NMDA receptors are widely studied in glutamatergic neurotransmission, the role of NMDA receptors in oligodendrocytes has remained enigmatic (De Biase et al., 2011; Guo et al., 2012; Káradóttir et al., 2005; Li et al., 2013; Lipton, 2006; Lundgaard et al., 2013; Micu et al., 2006; Piña-Crespo et al., 2010; Salter and Fern, 2005; Yang et al., 2014). In myelin, NR1

is associated with NR2C and NR3A subunits that provide a weak Mg^{2+} block (Burzomato et al., 2010; Das et al., 1998), suggesting that calcium entry does not require prior membrane depolarization. In development, NMDA receptors are most abundant in oligodendrocyte precursors (De Biase et al., 2010; Zhang et al., 2014). Unfortunately, the early functions of glutamate signaling were not revealed by the deletion of NR1 in OPC (De Biase et al., 2011; Guo et al., 2012). It is possible that calcium permeable AMPA receptors compensate functions other than GLUT1 trafficking, which is specifically regulated by NMDA receptor signaling. This is reminiscent of hippocampal LTP, which also requires NMDA receptors and is not compensated by AMPA receptors alone (Tsien et al., 1996).

Oligodendroglial NMDA receptors are localized in specialized microdomains of myelinating processes (Stirling and Stys, 2010; Stys, 2011) and also face the periaxonal space (Micu et al., 2006). Is NMDA receptor-dependent regulation of GLUT1 in oligodendrocytes and the non-compacted myelin compartment the same as GLUT4 regulation in other cell types (Bogan and Kandror, 2010)? In adipocytes, insulin-dependent GLUT4 trafficking requires calcium-dependent myosin motors (Yip et al., 2008). We were unable to mobilize GLUT1 with insulin in oligodendrocytes, but when triggered with NMDA, trafficking was expectedly calcium dependent and required a stable microtubule network (data not shown).

With the completion of developmental myelination, glycolysis products become gradually available to support the axonal energy metabolism, which is presumably more critical for fibers with high spiking activity. The ultrastructure of mature myelin is complex with narrow (non-compacted) cytosolic compartments in which glycolysis can take place. Once incorporated into these myelin membranes, glucose transporters are more likely to serve long-term functions than fast (“insulin-like”) adaptations to changing energy needs. Indeed, our ex vivo experiment showed that it takes many hours for oligodendrocytes to metabolically respond to the loss of glutamate signaling. However, activity-dependent regulation of axonal energy metabolism may be clinically relevant, e.g., in the aging brain or in neurodegenerative diseases (“use it or lose it”).

It is therefore of interest that NR1 mutant mice, when kept in standard housing (i.e., without physical challenges), showed signs of neurodegeneration beginning in the medulla and spinal cord at 10 months of age and progressing later to all CNS white matter tracts. Here, visible axonopathy and inflammation are most likely a “tip of the iceberg,” reflecting reduced energy metabolism in (many more) myelinated axons in vivo.

Finally, we note that astrocytes can also support axon function by releasing lactate in the white matter. They have direct access to the vasculature, store glycogen, and rapidly respond to energy deprivation with glycogen breakdown (Brown and Ransom, 2007). Theoretically, astrocytes may compensate some metabolic functions in oligodendroglial NMDA receptor mutants. The regulated metabolic interactions between axons, oligodendrocytes, and astrocytes are increasingly recognized as key for normal white matter function and likely for axon survival in many neurodegenerative diseases.

EXPERIMENTAL PROCEDURES

Mouse Strains

Female *Cnp1*-Cre mice (RRID: MGI_3051754) (Lappe-Siefke et al., 2003) were crossbred to floxed NR1 (gene symbol *Grin1*) mice (RRID: MGI_2175051) (Tsien et al., 1996). Conditional knockout animals were $Grin1^{flox/flox}{*}Cnp1^{Cre/+}$ mice. As controls, we used $Cnp1^{Cre/+}$, $Grin1^{flox/flox}{*}Cnp1^{+/+}$, or $Grin1^{flox/+}{*}Cnp1^{Cre/+}$ mice obtained as respective littermates. Some of the mice also carried the R26-stop-EYFP reporter gene for Cre activity (RRID: IMSR_JAX:006148) (Srinivas et al., 2001). Mice were maintained on the C57Bl6 background. Experiments were carried out mainly on male mice. Animal experiments were performed according to German, Spanish, and European guide lines for Animal Experimentation.

Cell Culture Preparation

Primary mouse or rat oligodendrocyte progenitor cells (OPCs) were isolated from cerebral cortices at P0–P2 as described previously (Barros et al., 2009; McCarthy and de Vellis, 1980). Cells were grown in DMEM (Lonza) supplemented with 10% fetal calf serum, Glutamax (Invitrogen), Penicillin and Streptomycin (Invitrogen) at 37°C, and 5% CO_2. Following OPC isolation, cells were differentiated for 5 days in Sato’s medium. For all experiments, Glutamax was withdrawn from the growth medium in the last 12–16 hr of differentiation. OPCs utilized for biotinylation assays, 2-deoxyglucose uptake, or lactate release were further purified to 98.2% ± 0.3% by negative selection immunopanning (Barres et al., 1992).

Immunocytochemistry

For GLUT1 and MCT1 immunocytochemistry, differentiated cells were treated for 30 min at 37°C with 100 μM NMDA. Glycine as co-agonist for NMDA receptors was already present in the medium. NMDA receptor blockers D-AP5 and/or 7CKA (100 μM) were applied 30 min prior to NMDA stimulation. Plasma membranes of mature oligodendrocytes were labeled with anti-galactocerebroside (GalC) antibody (Millipore Cat# MAB342 RRID: AB_94857) for 15 min at 37°C prior to fixation with 4% paraformaldehyde for 10 min at RT. Cells were permeabilized with ice-cold methanol for 5 min, washed with PBS, and incubated with anti-GLUT1 antibody (Abcam Cat# ab32551 RRID: AB_732605) or with anti-MCT1 (Millipore Cat# AB1286 RRID: AB_90565) overnight at 4°C. Analysis was carried out on confocal stacks of individual cells using ImageJ (http://rsb.info.nih.gov/ij/). Data are presented as the ratio of GLUT1 or MCT1 signal area to GalC area. Three individual experiments with 14–24 cells per condition were analyzed. Data were grouped per experiment and normalized to control condition.

Cell Surface Biotinylation

Immunopanned oligodendrocytes were treated with NMDA receptor agonists or antagonists as described above. Cell surface-associated proteins were labeled by incubation with 0.5 mg/ml membrane-impermeable EZ-link Sulfo-NHS-Biotin (Thermo Scientific) at 4°C for 30 min. After removing unbound biotin, cells were lysed for 15 min on ice with 1% Triton X-100, 0.2% SDS in PBS (pH 7.4) containing protease/phosphatase inhibitors. To isolate biotinylated proteins, 350–450 μg of lysate was incubated overnight at 4°C with 150 μl of 50% Pierce Streptavidin Agarose Resin in PBS (pH 7.2). After elution of biotinylated material, proteins were resolved by SDS-PAGE and immunoblotted with anti-GLUT1 or anti-MCT1 antibodies as described below.

Glucose Sensor Imaging

Rat mixed glial cells (after 8–12 days in culture) were transfected (using Fugene HD, Roche) with glucose sensor FLII12Pglu-700μΔ6 (Takanaga et al., 2008; Addgene plasmid 17866). 1 day after transfection, OPCs were isolated and further cultivated for 5 days. For details on FRET imaging, see Supplemental Information. NMDA receptor agonists and antagonists (each 100 μM) were applied, and FRET changes were analyzed. For control experiments and sensor calibration (Bittner et al., 2010), cells were incubated without glucose or adding either iodoacetate (glycolysis inhibitor, 1 mM) or cytochalasin B (glucose transporter blocker, 40 μM).

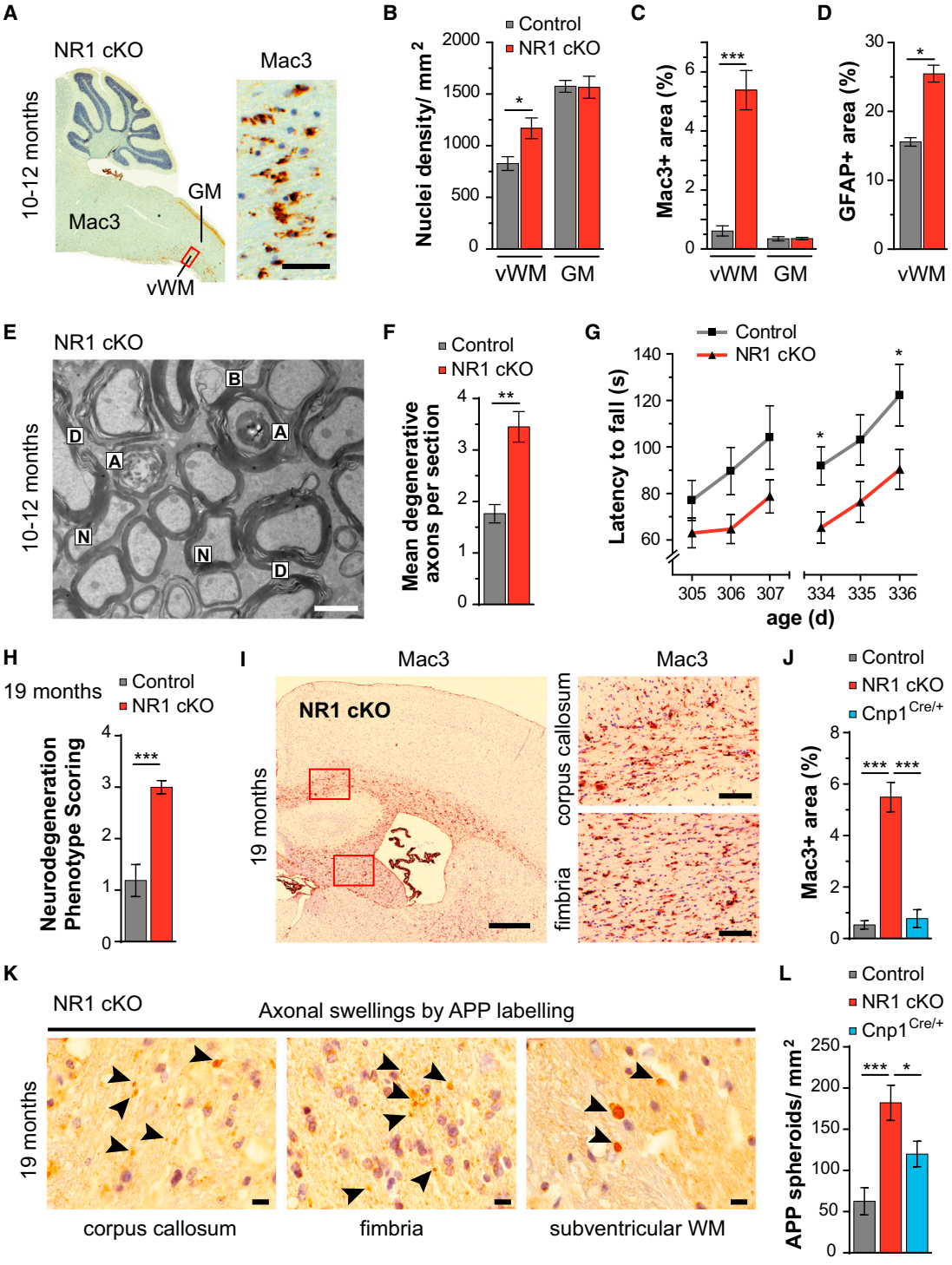

Figure 6. Late-Onset Neuroinflammation and Axonopathy in NR1 cKO Mice

(A) Indirect signs of neurodegeneration in white matter tracts at 1 year of age and overview (left) of sagittal cerebellum-spinal cord section from NR1 cKO mice. Signs of local inflammation (Mac3 immunostaining) were more obvious in the ventral white matter (vWM) compared to spinal cord gray matter (GM). Higher magnification (region marked by a red rectangle) reveals activated microglia (Mac3). Scale bar, 20 μm. See also Figure S7.

(B) Neuroinflammation in the ventral white matter of NR1 cKO mice confirmed by increased density of cell nuclei ($p = 0.029$, $n = 4$, Student's t test). In adjacent GM, nuclear densities are unaltered.

(C) Quantification of the $Mac3^+$ immunostained area (microgliosis) in vWM of NR1 mutant mice ($p = 0.0004$, $n = 4$, Student's t test)

(D) Quantification of the $GFAP^+$ area (astrogliosis) in vWM of NR1 mutant mice ($p = 0.013$, Student's t test).

(legend continued on next page)

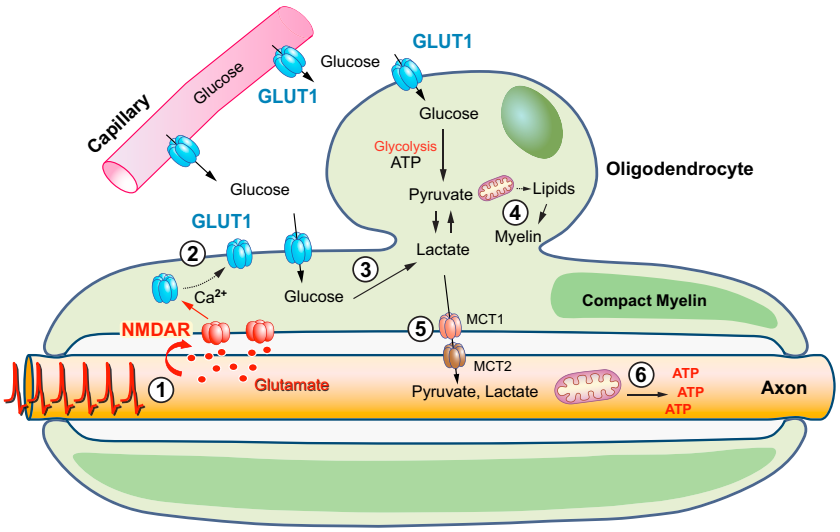

Figure 7. Schematic Depiction of Oligodendroglial NMDA Receptor Signaling

Working model in which axonal electrical activity in developing white matter tracts constitutes a glutamatergic signal for the surrounding OPC/oligodendrocytes/myelin compartments (1). After myelination, NMDA receptors associated with the internodal/paranodal membrane respond to axonal glutamate release as a surrogate marker for increased axonal electrical activity and energy needs, causing (2) the incorporation of additional glucose transporters into oligodendrocytes and myelin and the adaptation of glucose uptake (feed-forward regulation). Glycolysis products (3) are initially used for ATP and lipid synthesis (4). Later, mature oligodendrocytes release lactate (or pyruvate) to fuel the axonal compartment (5) for mitochondrial ATP production (6). Regulation of oligodendroglial glucose uptake by axonal energy needs could help prevent abnormal accumulation of lactate. The possible effect of glutamate on glucose transporters on astrocytes is not shown.

2-Deoxyglucose Uptake Measurements

Immunopanned oligodendrocytes differentiated for 5 days were incubated for 25 min in the presence or absence of NMDA/Gly (100 μM) in a modified medium (in mM: NaCl 91.17; KCl 5.37; NaH_2PO_4 0.91; Na_2HPO_4 0.23; $NaHCO_3$ 17.86; $MgSO_4$ 0.81; $CaCl_2$ 1.8; NaOH 16.7; HEPES 20; glucose 10; adjusted to pH 7.4 with HCl after equilibration with 5% CO2). Then glucose was replaced by 10 mM 2-deoxyglucose (2DG) for 5 min. 2-deoxyglucose-6-phosphate present within the cells was quantified using a commercial kit according to the instructions of the manufacturer (Cosmobio).

Measurements of Lactate Release by NMR

Immunopanned oligodendrocytes were differentiated for 4 days in Sato's medium containing 25 mM unlabeled glucose and for an additional day in Sato's medium containing 25 mM U-$^{13}C_6$-glucose. 100 μM NMDA/Gly was added for 30 min at 37°C in modified medium (see above) containing U-$^{13}C_6$-glucose. Conditioned media was immediately collected and snap frozen until NMR analysis. For details on NMR analysis, see Supplemental Information.

Immunohistochemistry

For NR1 labeling, mice were perfused with ice-cold artificial cerebrospinal fluid (ACSF). Optic nerves were isolated and immersion fixed with 4% PFA for 2 hr at RT and prepared for later cryo-sectioning. Slide-mounted sections (12 μm) were air-dried at RT and then treated with 0.3% Triton X-100 and 5% horse serum for 1 hr. Primary antibodies for NR1 (1:250, Millipore Cat# MAB363, RRID: AB_94946) and MBP (1:300, rabbit, Dako) were incubated overnight at 4°C in the same solution. Secondary antibodies were incubated in 2% horse serum for 2 hr at RT.

For analysis of local inflammation and pathology, paraffin sections of perfusion-fixed tissues were used. Sections were treated with primary antibodies diluted in PBS/BSA (1% w/v BSA) overnight at 4°C. Dilutions were as follows: GFAP (1:200, mouse, Novocastra), Mac3 (1:400, rat, BD PharMingen), and APP (1:1000, Millipore Cat# MAB348 RRID: AB_94882). Biotinylated secondary antibodies were then incubated for 30 min at RT, and chromogenic staining was completed using HRP-DAB detection.

Protein Analysis

Protein lysates of optic nerves from individual mice were prepared using the Precellys Ceramic Kit 1.4 mm and the Precellys 24 homogenizer (Peqlab). Nerves were homogenized in 150 μl sucrose buffer (in mM: 320 sucrose, 10 Tris [pH 7.4], 1 $NaHCO_3$, and 1 $MgCl_2$) and protease inhibitors (Complete tablets, Roche). For Western blotting, 30 μg protein lysate was size-separated on 12% SDS-polyacrylamide gels and blotted onto nitrocellulose membranes following instructions from BioRad. Primary antibodies to NR1 (1:500, Millipore Cat# MAB363, RRID: AB_94946) and GAPDH (1:2000, Enzo Life Sciences Cat# ADI-CSA-335-E, RRID: AB_2039148) were diluted in blocking buffer (5% milk) and incubated overnight at 4°C. Membranes were washed in 0.05% Tween prepared in phosphate buffer (PBS-T) followed by incubation with a horseradish peroxidase-conjugated secondary antibody. Proteins were detected with an enhanced chemiluminescence kit (Western Lightning, PerkinElmer) according to the manufacturer's instructions. Exposed ECL films (Amersham Biosciences) were scanned at grayscale (300 dpi resolution) using

(E and F) By electron microscopy of ventral cervical spinal cord cross sections (E), ultrastructural features of axonal pathology and degeneration were more frequent in NR1 mutant mice compared to controls (F) (n = 4–5 mice with 12–14 randomly taken images, covering 530 μm^2 each, p = 0.0014, Student's t test). Scale bar, 2 μm. In (E): A, axonal degeneration; B, blebbing membranes; D, delamination; N, normal myelin.

(G) Motor deficits of NR1 cKO mutants at 10−11 months of age, demonstrated by Rotarod testing on three consecutive days (repeated the following month). The latency to fall is decreased in NR1 mutant mice (red line) compared to littermate controls ($F_{genotype}$ (1, 17) = 4.95, p = 0.040, n = 9–10, two-way ANOVA).

(H) At age 19 months, NR1 cKO mice (n = 11) display significant neurological deficits compared to controls (n = 8, p < 0.001 Student's t test). Clinical scores are 0, asymptomatic; 1, hind limb clasping; 2, additionally, hunchback visible; 3, additionally, frequent slipping while walking on grid; 3.5, additionally, failure to hold on inverted grid; 4, additionally, hind limb ataxia and unable to hold on upright grid; 4.5, spastic hind limbs.

(I) Brain sections of 19-month-old NR1 cKO mice immunostained for $Mac3^+$ show widespread signs of neuroinflammation in white matter tracts; corpus callosum and fimbria are magnified (right panel).

(J) Quantification of $Mac3^+$ immunostained area in NR1 mutants compared to littermate controls and age-matched $Cnp1^{Cre/+}$ mice (n = 4–6 mice, p < 0.001, linear mixed effects analysis with post hoc Tukey correction for multiple comparisons).

(K) Axonopathy in white matter tracts revealed by APP immunolabeling (arrow heads) in brain sections of 19-month-old NR1 cKO mice; corpus callosum, fimbria, and subventricular white matter are shown.

(L) Quantification of APP spheroids in NR1 mutants in comparison to littermate controls and age-matched $Cnp1^{Cre/+}$ mice (n = 4–6 mice; control versus NR1 cKO p < 0.001 and $Cnp1^{Cre/+}$ versus NR1 cKO p = 0.03, linear mixed effects analysis with post hoc Tukey correction for multiple comparisons).

a regular image scanner, followed by densitometric analysis with ImageJ. The peak intensity for NR1 was normalized to the peak intensity of GAPDH.

Immunoelectron Microscopy

Freshly dissected optic nerves were immersion fixed with 4% formaldehyde and 0.2% glutaraldehyde in 0.1 M phosphate buffer containing 0.5% NaCl. After embedding in 10% gelatine and subsequent infiltration with 2.3 M sucrose in 0.1 M PB overnight, small blocks of gelatin containing optic nerve pieces were mounted onto aluminum pins for ultramicrotomy and frozen in liquid nitrogen. Ultrathin cryosections were picked up with a 1:1 mixture of 2% methylcellulose and 2.3 M sucrose. Sections were incubated with antibodies against GLUT1 (1:100, Abcam Cat# ab32551 RRID: AB_732605) and MCT1 (1:1,000, Millipore Cat# AB1286 RRID: AB_90565) and detected with protein A-gold (10 nm, obtained from the Cell Microscopy Center, Department of Cell Biology, University Medical Center Utrecht, NL), and by anti-chicken immunogold (10 nm, Aurion), respectively. Sections were analyzed with a LEO EM912AB (Zeiss), and digital micrographs were obtained with an on-axis 2048×2048-CCD camera (TRS, Moorenweis). For quantification, 10–12 randomly taken images from three controls and three NR1 mutants were assessed. Per image, all myelinated axons and immunogold particles associated with myelinated axons were counted, and a ratio of immunogold particles to the number of myelinated axons was calculated. The mean ratio per animal was then normalized to controls.

Myelin Preparation and Immunoblotting

Myelin was purified as described before (Norton and Poduslo, 1973) from mouse brain homogenate in 0.32 M sucrose. Immunoblotting was performed as described before (Werner et al., 2007). Briefly, 30 μg of protein were separated on 10% SDS-polyacrylamide gels, blotted onto polyvinylidene difluoride membranes (Roche), and incubated with primary antibodies for GLUT1 (1:500, Abcam Cat# ab32551 RRID: AB_732605), MCT1 (1:1,000, Millipore Cat# AB1286 RRID: AB_90565), and SIRT2 (1:2,000) (Dryden et al., 2003). Blots were incubated with horseradish peroxidase-coupled secondary antibodies (Dianova) and developed by enhanced chemiluminescence (Western Lightning ECL, PerkinElmer) using a luminescence imager (Intas).

Electron Microscopy and Morphometry

Optic nerves were acutely removed and either immersion-fixed for conventional sample preparation or cryofixed by HPF and freeze substituted as described in detail (Möbius et al., 2010). For analysis of axonal pathology, animals were perfusion-fixed (4% formaldehyde, 2.5% glutaraldehyde). For structural analysis of optic nerves that were subjected to OGD, nerves were directly immersion-fixed (4% formaldehyde, 2.5% glutaraldehyde). For analysis of unmyelinated, myelinated, and ensheathed axons (defined as 1–3 uncompacted layers), 4–6 EM images with 12,000× magnification 400–700 axons were counted for each nerve. Data were grouped per animal. For g-ratio analysis, 4–5 random overview pictures were taken at 8,000× magnification, 200 axons analyzed using ImageJ (images were blinded for experimenter). G-ratios (axonal diameter divided by the fiber diameter including the myelin sheath) were calculated from circular areas equivalent to the measured areas of axons and myelin sheath including the axon.

Optic Nerve Recordings

Following anesthesia and decapitation, nerves were gently removed, placed into an interface perfusion chamber (Haas Top, Harvard Apparatus), and superfused with ACSF containing the following (in mM): 124 NaCl, 3.0 KCl, 2.0 $CaCl_2$, 2.0 $MgSO_4$, 1.25 NaH_2PO_4, 23 $NaHCO_3$, and 10 glucose. Perfusion chamber was continuously aerated by a humidified gas mixture of 95% O_2/5% CO_2, and experiments were performed at 37°C.

For oxygen-glucose deprivation (OGD), the protocol was performed as described previously (Baltan et al., 2008). CAPs were elicited every 30 s, and OGD (applied for 60 min) was induced by switching to glucose-free ACSF and a gas mixture containing 95% N_2/5% CO_2. After OGD control ACSF and O_2 were restored and CAPs were recorded for up to 2–3 hr, responses were stabilized within 20 to 30 min. When L-Lactate (20 mM, Sigma) was used during recovery, it was substituted for 20 mM NaCl.

CAP area is proportional to the total number of excited axons (Stys et al., 1991). Irreversible injury was measured by determining residual CAP area 1.5–2 hr after conclusion of OGD, normalized to baseline CAP area.

For the long-term ex vivo analysis, wild-type nerves were continuously superfused with ACSF containing either NMDA and glycine (NMDA/Gly 100 μM), NMDA/Gly plus 7CKA and D-AP5 (7CKA/D-AP5 100 μM), or DMSO only (DMSO Control). After 16 hr of treatment, CAPs were recorded at 0.2 Hz to obtain baseline, and then nerves were challenged with a gradual increase in stimulation frequency (from 1 to 100 Hz), with each stimulus train lasting 30 s. For 1 and 5 Hz stimulations, CAPs were continuously recorded. For 10, 25, 50, and 100 Hz stimulations, CAPs were sampled after a burst of each 100 stimuli with an inter-burst interval of 300 ms. CAP area of the graded responses were analyzed for each treatment group (2.1 ms after stimulus onset) and normalized to baseline.

In Vivo Spinal Cord CAP Recordings

For details, see Supplemental Information. Stimulation and recording from spinal cord axons in vivo were performed with bipolar platinum electrodes. Square-wave constant voltage pulses (100 μs) were used to stimulate the dorsal root L4, and CAPs were recorded from the ipsilateral fasciculus gracilis at spinal cord level L1. Dorsal roots were stimulated at different frequencies (0.1, 10, and 100 Hz), and CAP recordings were sampled at 50 kHz. Distance between the electrodes was measured using a thin cotton thread to evaluate conduction velocities. For analysis of axonal firing strength, the peak-to-peak amplitude (of the first and most robust peak of the CAP recording) was monitored over time and normalized to baseline (0.1 Hz).

Rotarod and Clinical Score

Mice (10–12 months) were placed on a horizontal rod at 1 rpm and accelerated with 1 rpm every 10 s (three tests per trial). The clinical scores at the age of 19 months were as follows: 0, asymptomatic; 1, hind limb clasping; 2, additionally, hunchback visible; 3, additionally, slipping during walking on a grid; 3.5, additionally, not able to hold on an inverted grid; 4, additionally, hind limb ataxia, not able to hold on an upright grid and reduced righting reflex; 4.5, spastic hind limbs.

Statistical Analysis

Inter-group comparisons were done by Mann Whitney t test or two-tailed Student's t test. For multiple comparisons, data were analyzed with one-way or two-way ANOVA with Bonferroni's post-test or using linear mixed effects models (lme4 package v.1.1.9; https://cran.r-project.org/web/packages/lme4/). All analyses were conducted through GraphPad Prism 4 or R (v.3.2.2, R Core Team, 2015). The levels of significance were set as *$p < 0.05$; **$p < 0.01$; ***$p < 0.001$. Data are represented as means ± SEM.

SUPPLEMENTAL INFORMATION

Supplemental Information includes Supplemental Experimental Procedures and seven figures and can be found with this article online at http://dx.doi.org/10.1016/j.neuron.2016.05.016.

AUTHOR CONTRIBUTIONS

All authors analyzed data and contributed ideas to the manuscript. A.S.S. performed mouse breeding experiments, histology, qPCR and protein analysis, microscopy, optic nerve recordings, and EM analysis. S.B., A.S.S., and A.T. performed optic nerve recordings; culture experiments and FRET sensor imaging were performed by J.H., I.D.T., A.T., and A.S.S.; NMR measurements and analysis were performed by D.B. and C.G.; W.M. performed HPF-EM and immuno-EM analyses; P.D., H.S., and E.D.S. performed in vivo spinal cord recordings; K.K. performed myelin preparations, protein analysis, and neurological scoring of aged mice; B.G. and S.L. performed behavioral assessment of visual performance; H.M.J. helped with EM analysis; W.H. contributed to optic nerve protein analysis; A.P.-S., F.P.-C. and C.M. performed EAE analysis; F.K. and K.-A.N. supervised the project; A.S.S. and K.-A.N. wrote the manuscript.

ACKNOWLEDGMENTS

We thank M.J. Barrett for help in statistical analyses. We thank T. Ruhwedel, A. Fahrenholz, U. Bode, F. Rhode, O. López, and H. Gómez for technical assistance, D. Rhode and C. Casper for animal husbandry, and B. Hamprecht for helpful discussions. This work was supported by the DFG (Research Center Molecular Physiology of the Brain/CNMPB to K.-A.N, F.K., W.M., and C.G.), DFG SPP-1757 (K.-A.N.), NIH/NIA Grant AG033720 and the American Heart Association National Scientist Development Grant (S.B.), Ministerio de Ciencia e Innovación (grant no. SAF2013-45084-R) and CIBERNED (C.M.), DFG SPP-1172 (F.K. and K.-A.N.), DFG SFB 894 (F.K.), DFG SFB/Transregio TRR43 (K.-A.N. and F.K.), European Commission FP7-202167 NeuroGLIA (F.K.), and an ERC Advanced Investigators Grant (K.-A.N.). A.S.S. is supported by a long-term EMBO fellowship.

Received: November 12, 2015
Revised: March 11, 2016
Accepted: May 5, 2016
Published: June 9, 2016

REFERENCES

Baltan, S., Besancon, E.F., Mbow, B., Ye, Z., Hamner, M.A., and Ransom, B.R. (2008). White matter vulnerability to ischemic injury increases with age because of enhanced excitotoxicity. J. Neurosci. *28*, 1479–1489.

Barres, B.A., Hart, I.K., Coles, H.S., Burne, J.F., Voyvodic, J.T., Richardson, W.D., and Raff, M.C. (1992). Cell death and control of cell survival in the oligodendrocyte lineage. Cell *70*, 31–46.

Barros, C.S., Nguyen, T., Spencer, K.S., Nishiyama, A., Colognato, H., and Müller, U. (2009). Beta1 integrins are required for normal CNS myelination and promote AKT-dependent myelin outgrowth. Development *136*, 2717–2724.

Barry, J.M. (2015). Axonal activity in vivo: technical considerations and implications for the exploration of neural circuits in freely moving animals. Front. Neurosci. *9*, 153.

Bittner, C.X., Loaiza, A., Ruminot, I., Larenas, V., Sotelo-Hitschfeld, T., Gutiérrez, R., Córdova, A., Valdebenito, R., Frommer, W.B., and Barros, L.F. (2010). High resolution measurement of the glycolytic rate. Front. Neuroenergetics *2*, 2.

Bogan, J.S., and Kandror, K.V. (2010). Biogenesis and regulation of insulin-responsive vesicles containing GLUT4. Curr. Opin. Cell Biol. *22*, 506–512.

Brown, A.M., and Ransom, B.R. (2007). Astrocyte glycogen and brain energy metabolism. Glia *55*, 1263–1271.

Burzomato, V., Frugier, G., Pérez-Otaño, I., Kittler, J.T., and Attwell, D. (2010). The receptor subunits generating NMDA receptor mediated currents in oligodendrocytes. J. Physiol. *588*, 3403–3414.

Das, S., Sasaki, Y.F., Rothe, T., Premkumar, L.S., Takasu, M., Crandall, J.E., Dikkes, P., Conner, D.A., Rayudu, P.V., Cheung, W., et al. (1998). Increased NMDA current and spine density in mice lacking the NMDA receptor subunit NR3A. Nature *393*, 377–381.

De Biase, L.M., Nishiyama, A., and Bergles, D.E. (2010). Excitability and synaptic communication within the oligodendrocyte lineage. J. Neurosci. *30*, 3600–3611.

De Biase, L.M., Kang, S.H., Baxi, E.G., Fukaya, M., Pucak, M.L., Mishina, M., Calabresi, P.A., and Bergles, D.E. (2011). NMDA receptor signaling in oligodendrocyte progenitors is not required for oligodendrogenesis and myelination. J. Neurosci. *31*, 12650–12662.

Dryden, S.C., Nahhas, F.A., Nowak, J.E., Goustin, A.S., and Tainsky, M.A. (2003). Role for human SIRT2 NAD-dependent deacetylase activity in control of mitotic exit in the cell cycle. Mol. Cell. Biol. *23*, 3173–3185.

Emery, B. (2010). Regulation of oligodendrocyte differentiation and myelination. Science *330*, 779–782.

Ferreira, J.M., Burnett, A.L., and Rameau, G.A. (2011). Activity-dependent regulation of surface glucose transporter-3. J. Neurosci. *31*, 1991–1999.

Fünfschilling, U., Supplie, L.M., Mahad, D., Boretius, S., Saab, A.S., Edgar, J., Brinkmann, B.G., Kassmann, C.M., Tzvetanova, I.D., Möbius, W., et al. (2012). Glycolytic oligodendrocytes maintain myelin and long-term axonal integrity. Nature *485*, 517–521.

Gibson, E.M., Purger, D., Mount, C.W., Goldstein, A.K., Lin, G.L., Wood, L.S., Inema, I., Miller, S.E., Bieri, G., Zuchero, J.B., et al. (2014). Neuronal activity promotes oligodendrogenesis and adaptive myelination in the mammalian brain. Science *344*, 1252304.

Griffiths, I., Klugmann, M., Anderson, T., Yool, D., Thomson, C., Schwab, M.H., Schneider, A., Zimmermann, F., McCulloch, M., Nadon, N., and Nave, K.A. (1998). Axonal swellings and degeneration in mice lacking the major proteolipid of myelin. Science *280*, 1610–1613.

Guo, F., Maeda, Y., Ko, E.M., Delgado, M., Horiuchi, M., Soulika, A., Miers, L., Burns, T., Itoh, T., Shen, H., et al. (2012). Disruption of NMDA receptors in oligodendroglial lineage cells does not alter their susceptibility to experimental autoimmune encephalomyelitis or their normal development. J. Neurosci. *32*, 639–645.

Hamilton, N.B., Kolodziejczyk, K., Kougioumtzidou, E., and Attwell, D. (2016). Proton-gated Ca(2+)-permeable TRP channels damage myelin in conditions mimicking ischaemia. Nature *529*, 523–527.

Hildebrand, C., and Waxman, S.G. (1984). Postnatal differentiation of rat optic nerve fibers: electron microscopic observations on the development of nodes of Ranvier and axoglial relations. J. Comp. Neurol. *224*, 25–37.

Káradóttir, R., Cavelier, P., Bergersen, L.H., and Attwell, D. (2005). NMDA receptors are expressed in oligodendrocytes and activated in ischaemia. Nature *438*, 1162–1166.

Kassmann, C.M., Lappe-Siefke, C., Baes, M., Brügger, B., Mildner, A., Werner, H.B., Natt, O., Michaelis, T., Prinz, M., Frahm, J., and Nave, K.A. (2007). Axonal loss and neuroinflammation caused by peroxisome-deficient oligodendrocytes. Nat. Genet. *39*, 969–976.

Kukley, M., Capetillo-Zarate, E., and Dietrich, D. (2007). Vesicular glutamate release from axons in white matter. Nat. Neurosci. *10*, 311–320.

Lappe-Siefke, C., Goebbels, S., Gravel, M., Nicksch, E., Lee, J., Braun, P.E., Griffiths, I.R., and Nave, K.A. (2003). Disruption of Cnp1 uncouples oligodendroglial functions in axonal support and myelination. Nat. Genet. *33*, 366–374.

Lee, Y., Morrison, B.M., Li, Y., Lengacher, S., Farah, M.H., Hoffman, P.N., Liu, Y., Tsingalia, A., Jin, L., Zhang, P.W., et al. (2012). Oligodendroglia metabolically support axons and contribute to neurodegeneration. Nature *487*, 443–448.

Li, C., Xiao, L., Liu, X., Yang, W., Shen, W., Hu, C., Yang, G., and He, C. (2013). A functional role of NMDA receptor in regulating the differentiation of oligodendrocyte precursor cells and remyelination. Glia *61*, 732–749.

Lipton, S.A. (2006). NMDA receptors, glial cells, and clinical medicine. Neuron *50*, 9–11.

Liu, J., Dietz, K., DeLoyht, J.M., Pedre, X., Kelkar, D., Kaur, J., Vialou, V., Lobo, M.K., Dietz, D.M., Nestler, E.J., et al. (2012). Impaired adult myelination in the prefrontal cortex of socially isolated mice. Nat. Neurosci. *15*, 1621–1623.

Lundgaard, I., Luzhynskaya, A., Stockley, J.H., Wang, Z., Evans, K.A., Swire, M., Volbracht, K., Gautier, H.O., Franklin, R.J., Attwell, D., and Káradóttir, R.T.; Charles Ffrench-Constant (2013). Neuregulin and BDNF induce a switch to NMDA receptor-dependent myelination by oligodendrocytes. PLoS Biol. *11*, e1001743.

Matute, C. (2010). Calcium dyshomeostasis in white matter pathology. Cell Calcium *47*, 150–157.

McCarthy, K.D., and de Vellis, J. (1980). Preparation of separate astroglial and oligodendroglial cell cultures from rat cerebral tissue. J. Cell Biol. *85*, 890–902.

Micu, I., Jiang, Q., Coderre, E., Ridsdale, A., Zhang, L., Woulfe, J., Yin, X., Trapp, B.D., McRory, J.E., Rehak, R., et al. (2006). NMDA receptors mediate calcium accumulation in myelin during chemical ischaemia. Nature *439*, 988–992.

Micu, I., Plemel, J.R., Lachance, C., Proft, J., Jansen, A.J., Cummins, K., van Minnen, J., and Stys, P.K. (2016). The molecular physiology of the axo-myelinic synapse. Exp. Neurol. *276*, 41–50.

Miller, R.H., David, S., Patel, R., Abney, E.R., and Raff, M.C. (1985). A quantitative immunohistochemical study of macroglial cell development in the rat optic nerve: in vivo evidence for two distinct astrocyte lineages. Dev. Biol. *111*, 35–41.

Möbius, W., Cooper, B., Kaufmann, W.A., Imig, C., Ruhwedel, T., Snaidero, N., Saab, A.S., and Varoqueaux, F. (2010). Electron microscopy of the mouse central nervous system. Methods Cell Biol. *96*, 475–512.

Morrison, B.M., Lee, Y., and Rothstein, J.D. (2013). Oligodendroglia: metabolic supporters of axons. Trends Cell Biol. *23*, 644–651.

Nave, K.A. (2010). Myelination and the trophic support of long axons. Nat. Rev. Neurosci. *11*, 275–283.

Nave, K.A., and Werner, H.B. (2014). Myelination of the nervous system: mechanisms and functions. Annu. Rev. Cell Dev. Biol. *30*, 503–533.

Norton, W.T., and Poduslo, S.E. (1973). Myelination in rat brain: method of myelin isolation. J. Neurochem. *21*, 749–757.

Perge, J.A., Niven, J.E., Mugnaini, E., Balasubramanian, V., and Sterling, P. (2012). Why do axons differ in caliber? J. Neurosci. *32*, 626–638.

Piña-Crespo, J.C., Talantova, M., Micu, I., States, B., Chen, H.S., Tu, S., Nakanishi, N., Tong, G., Zhang, D., Heinemann, S.F., et al. (2010). Excitatory glycine responses of CNS myelin mediated by NR1/NR3 "NMDA" receptor subunits. J. Neurosci. *30*, 11501–11505.

Rinholm, J.E., Hamilton, N.B., Kessaris, N., Richardson, W.D., Bergersen, L.H., and Attwell, D. (2011). Regulation of oligodendrocyte development and myelination by glucose and lactate. J. Neurosci. *31*, 538–548.

Saab, A.S., Tzvetanova, I.D., and Nave, K.A. (2013). The role of myelin and oligodendrocytes in axonal energy metabolism. Curr. Opin. Neurobiol. *23*, 1065–1072.

Salter, M.G., and Fern, R. (2005). NMDA receptors are expressed in developing oligodendrocyte processes and mediate injury. Nature *438*, 1167–1171.

Snaidero, N., Möbius, W., Czopka, T., Hekking, L.H., Mathisen, C., Verkleij, D., Goebbels, S., Edgar, J., Merkler, D., Lyons, D.A., et al. (2014). Myelin membrane wrapping of CNS axons by PI(3,4,5)P3-dependent polarized growth at the inner tongue. Cell *156*, 277–290.

Srinivas, S., Watanabe, T., Lin, C.S., William, C.M., Tanabe, Y., Jessell, T.M., and Costantini, F. (2001). Cre reporter strains produced by targeted insertion of EYFP and ECFP into the ROSA26 locus. BMC Dev. Biol. *1*, 4.

Stirling, D.P., and Stys, P.K. (2010). Mechanisms of axonal injury: internodal nanocomplexes and calcium deregulation. Trends Mol. Med. *16*, 160–170.

Stys, P.K. (2011). The axo-myelinic synapse. Trends Neurosci. *34*, 393–400.

Stys, P.K., Ransom, B.R., and Waxman, S.G. (1991). Compound action potential of nerve recorded by suction electrode: a theoretical and experimental analysis. Brain Res. *546*, 18–32.

Takanaga, H., Chaudhuri, B., and Frommer, W.B. (2008). GLUT1 and GLUT9 as major contributors to glucose influx in HepG2 cells identified by a high sensitivity intramolecular FRET glucose sensor. Biochim. Biophys. Acta *1778*, 1091–1099.

Tekkök, S.B., Brown, A.M., Westenbroek, R., Pellerin, L., and Ransom, B.R. (2005). Transfer of glycogen-derived lactate from astrocytes to axons via specific monocarboxylate transporters supports mouse optic nerve activity. J. Neurosci. Res. *81*, 644–652.

Tekkök, S.B., Ye, Z., and Ransom, B.R. (2007). Excitotoxic mechanisms of ischemic injury in myelinated white matter. J. Cereb. Blood Flow Metab. *27*, 1540–1552.

Tsien, J.Z., Huerta, P.T., and Tonegawa, S. (1996). The essential role of hippocampal CA1 NMDA receptor-dependent synaptic plasticity in spatial memory. Cell *87*, 1327–1338.

Wake, H., Lee, P.R., and Fields, R.D. (2011). Control of local protein synthesis and initial events in myelination by action potentials. Science *333*, 1647–1651.

Werner, H.B., Kuhlmann, K., Shen, S., Uecker, M., Schardt, A., Dimova, K., Orfaniotou, F., Dhaunchak, A., Brinkmann, B.G., Möbius, W., et al. (2007). Proteolipid protein is required for transport of sirtuin 2 into CNS myelin. J. Neurosci. *27*, 7717–7730.

Wyss, M.T., Jolivet, R., Buck, A., Magistretti, P.J., and Weber, B. (2011). In vivo evidence for lactate as a neuronal energy source. J. Neurosci. *31*, 7477–7485.

Yang, X., Hamner, M.A., Brown, A.M., Evans, R.D., Ye, Z.C., Chen, S., and Ransom, B.R. (2014). Novel hypoglycemic injury mechanism: N-methyl-D-aspartate receptor-mediated white matter damage. Ann. Neurol. *75*, 492–507.

Yip, M.F., Ramm, G., Larance, M., Hoehn, K.L., Wagner, M.C., Guilhaus, M., and James, D.E. (2008). CaMKII-mediated phosphorylation of the myosin motor Myo1c is required for insulin-stimulated GLUT4 translocation in adipocytes. Cell Metab. *8*, 384–398.

Zhang, Y., Chen, K., Sloan, S.A., Bennett, M.L., Scholze, A.R., O'Keeffe, S., Phatnani, H.P., Guarnieri, P., Caneda, C., Ruderisch, N., et al. (2014). An RNA-sequencing transcriptome and splicing database of glia, neurons, and vascular cells of the cerebral cortex. J. Neurosci. *34*, 11929–11947.

Ziskin, J.L., Nishiyama, A., Rubio, M., Fukaya, M., and Bergles, D.E. (2007). Vesicular release of glutamate from unmyelinated axons in white matter. Nat. Neurosci. *10*, 321–330.

Neuron, Volume *91*

Supplemental Information

Oligodendroglial NMDA Receptors Regulate Glucose Import and Axonal Energy Metabolism

Aiman S. Saab, Iva D. Tzvetavona, Andrea Trevisiol, Selva Baltan, Payam Dibaj, Kathrin Kusch, Wiebke Möbius, Bianka Goetze, Hannah M. Jahn, Wenhui Huang, Heinz Steffens, Eike D. Schomburg, Alberto Pérez-Samartín, Fernando Pérez-Cerdá, Davood Bakhtiari, Carlos Matute, Siegrid Löwel, Christian Griesinger, Johannes Hirrlinger, Frank Kirchhoff, and Klaus-Armin Nave

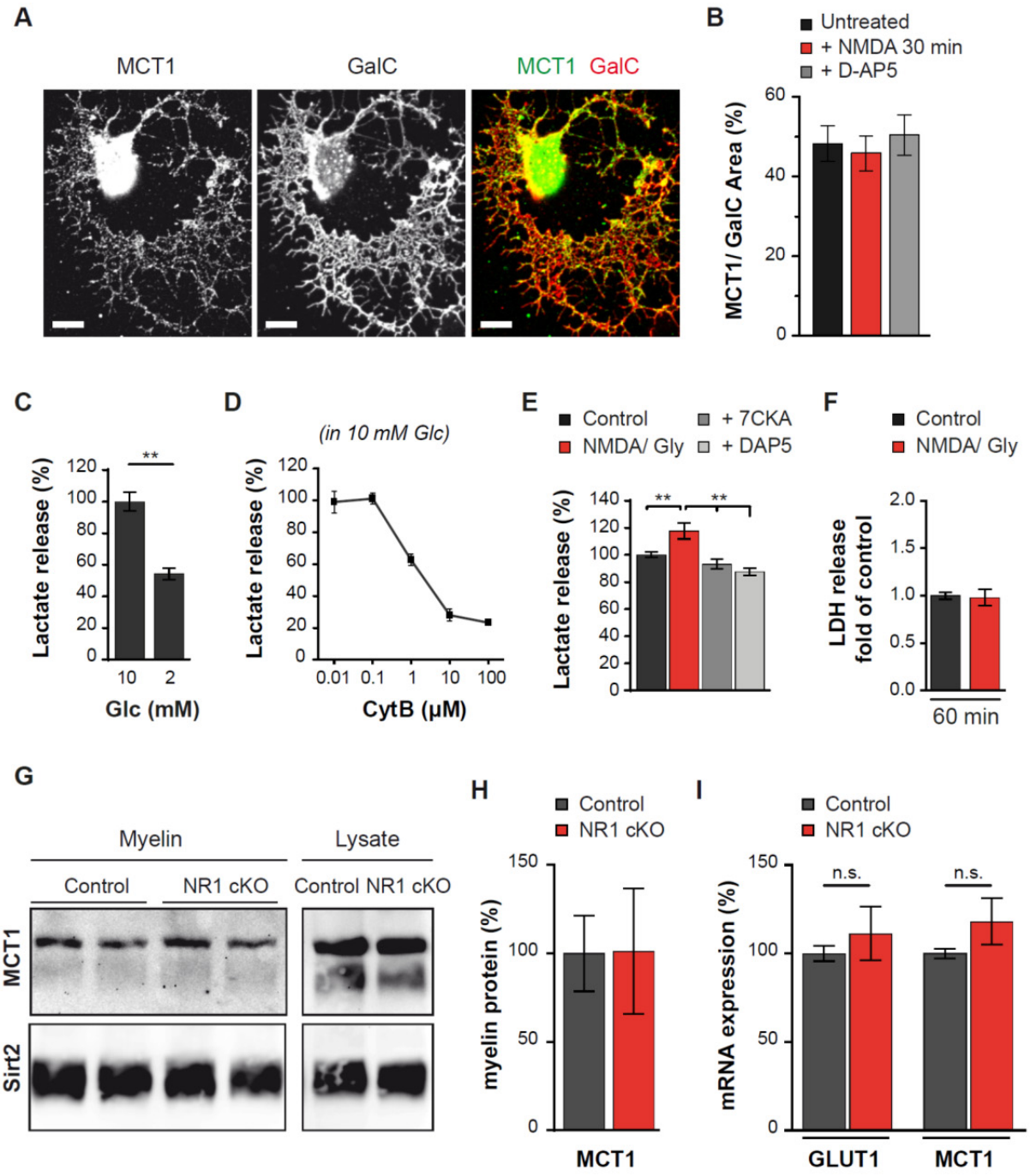

Figure S1 (Related to Figure 1 and 2). Oligodendroglial MCT1 expression is not altered by NMDA receptor stimulation in culture, lactate release from primary oligodendrocytes, and MCT1 abundance in myelin is unchanged in NR1 mutant mice.
A, **B** Immunolabelling of MCT1 in primary oligodendrocytes revealed readily detectable signals at the cell surface. NMDA receptor stimulation for 30 min did not cause any overt MCT1 redistribution, when quantified and normalized to GalC surface staining. Scale bar 10 µm.
C, Lactate release by cultured oligodendrocytes depends on glucose levels in the medium (note K_m for Glut1 is ~ 3 mM).
D, Dose-dependent inhibition by cytochalasin B (CytB), a glucose transporter blocker, reduces lactate release into the medium (containing 10 mM glucose) of oligodendrocytes.
E, Activation of NMDA receptors increases lactate release by 18 % ± 6 % compared to untreated conditions and is specifically blocked by 7CKA or D-AP5 (** $P < 0.01$, n = 5-6; Mann Whitney t test). 7CKA and D-AP5 were used to block the glycinerig and glutamatergic binding site of NMDA receptors, respectively.
F, Measurement of lactate dehydrogenase (LDH), 60 min after the addition of 100 µM NMDA/Gly to the culture medium, yields no evidence for oligodendrocyte death by excitotoxicity.
G, **H**, Western blot analysis of MCT1 in myelin and in total brain lysates from NR1 mutant and control brains. When quantified, MCT1 protein abundance in myelin is not different between NR1 mutants and controls. SIRT2 was used as a loading control
I, mRNA expression of GLUT1 and MCT1 was not significantly altered when comparing samples from enriched white matter of NR1 mutants and littermate controls.

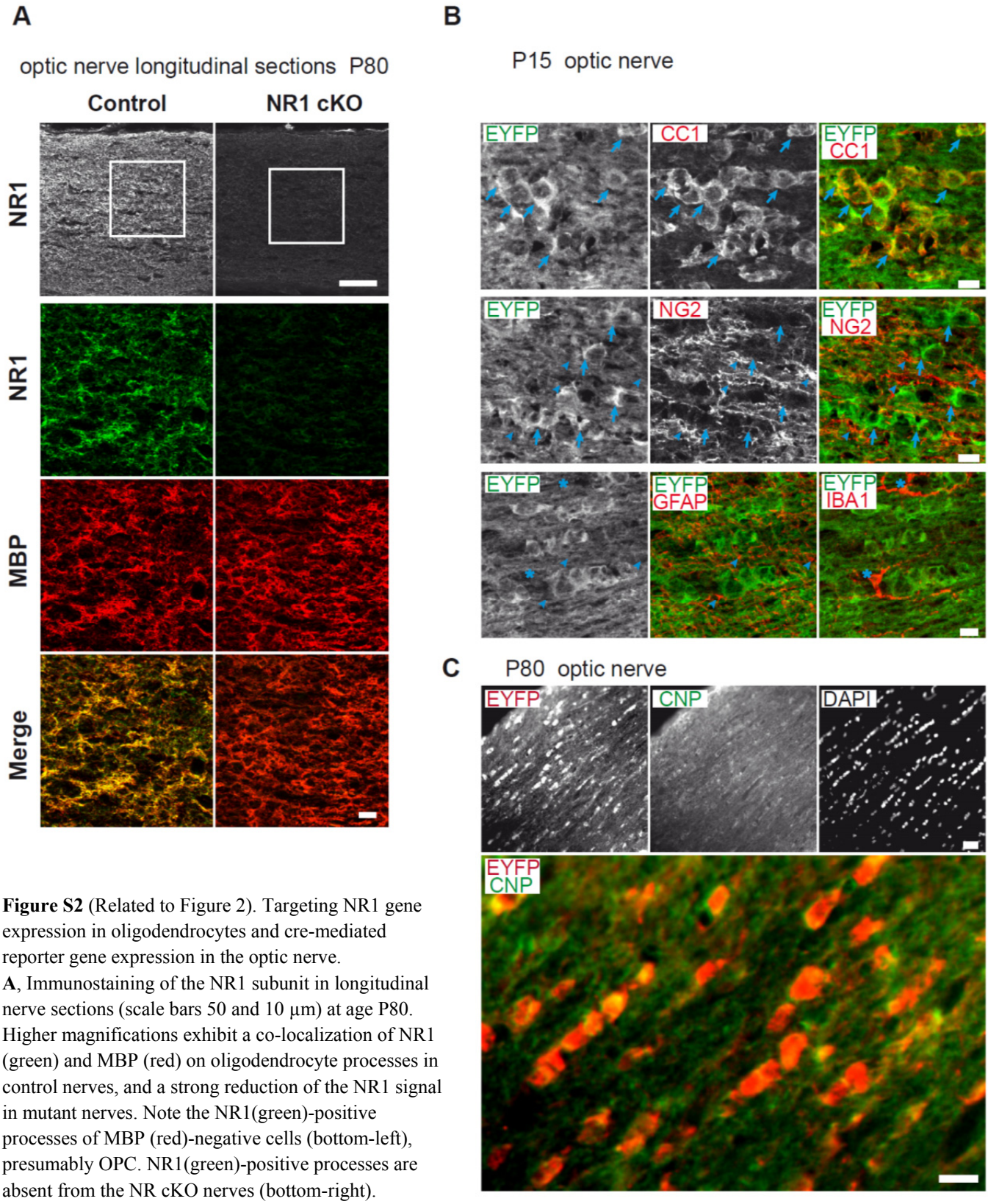

Figure S2 (Related to Figure 2). Targeting NR1 gene expression in oligodendrocytes and cre-mediated reporter gene expression in the optic nerve.

A, Immunostaining of the NR1 subunit in longitudinal nerve sections (scale bars 50 and 10 µm) at age P80. Higher magnifications exhibit a co-localization of NR1 (green) and MBP (red) on oligodendrocyte processes in control nerves, and a strong reduction of the NR1 signal in mutant nerves. Note the NR1(green)-positive processes of MBP (red)-negative cells (bottom-left), presumably OPC. NR1(green)-positive processes are absent from the NR cKO nerves (bottom-right).

B, Cnp1-Cre*ROSA26-floxed-STOP-EYFP mice reveal reporter gene expression in recombined cells of the optic nerve at P15. Confocal sections were immunostained for EYFP (with anti-GFP antibody to enhance reporter signal) and CC1 (mature oligodendrocytes), for EYFP and NG2 (OPCs), and for EYFP, GFAP (astrocytes) and IBA1 (microglia). Arrows indicate mature oligodendrocytes positive for EYFP and CC1. Arrowheads indicate OPC (immunostained for NG2, middle) or astrocytes (immunostained for GFAP, bottom) that are EYFP negative. Asterisks indicate microglia (immunostained for IBA1 but not EYFP). Scale bars 10 µm.

C, Reporter analysis at P80. Epifluorescent overview of longitudinal optic nerve section stained for EYFP and CNP (mature oligodendrocytes). DAPI staining labels nuclei. At higher magnification (bottom) there is a virtually complete overlap of EYFP reporter and CNP expression. Scale bars 20 µm (top), 10 µm (bottom).

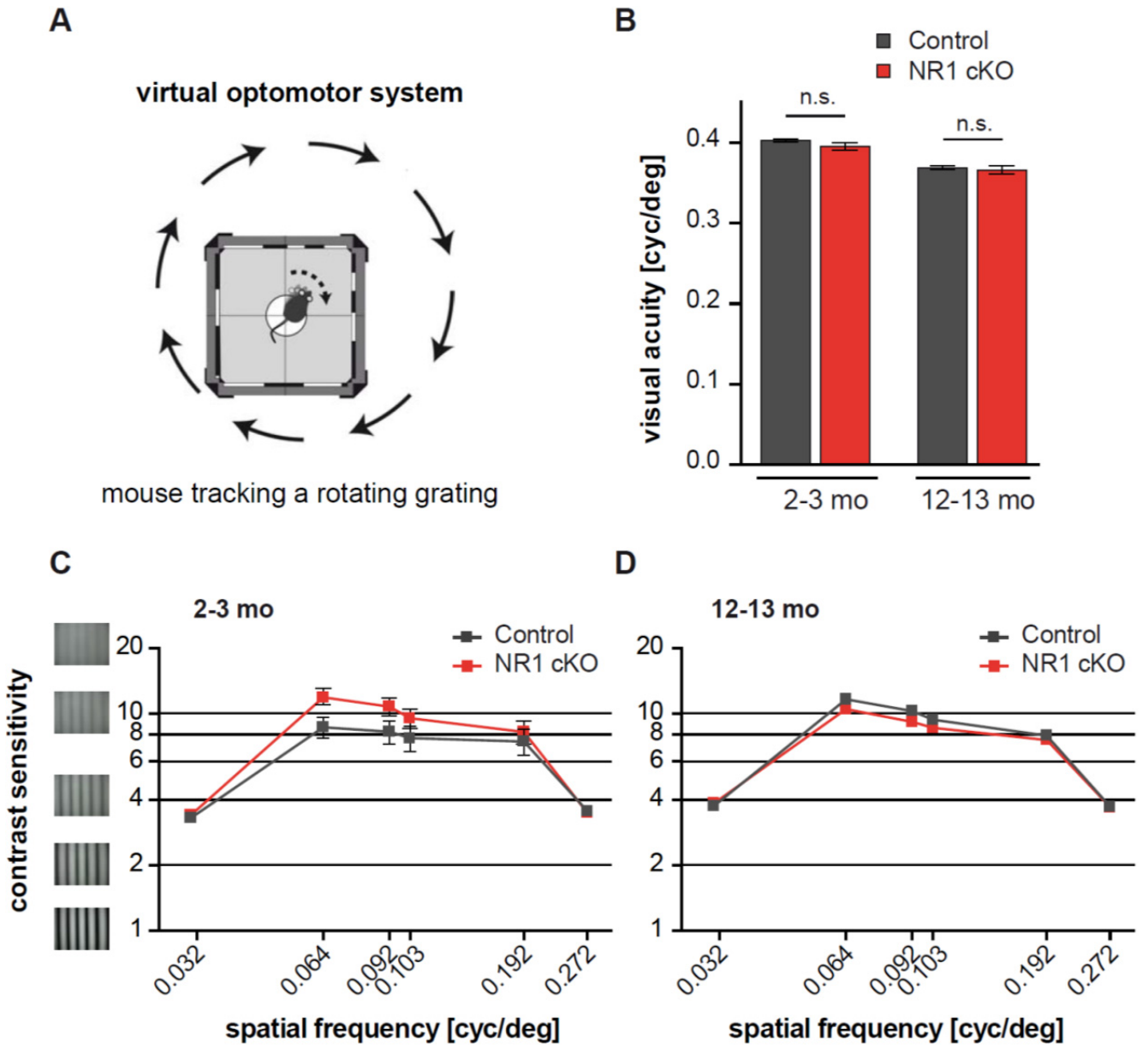

Figure S3 (Related to Figure 3). Behavioural assessment of visual acuity and contrast sensitivity.
A, Visual acuity and contrast sensitivity were measured with a virtual-reality optomotor system. Scheme modified from (Prusky et al., 2004) with permission.
B, Visual acuity was measured with moving gratings of increasing spatial frequency (in cycles per degree = cyc/deg), until the mice stopped tracking. NR1 mutant and littermate controls were examined at 2-3 months and at 12-13 months of age but revealed no difference of performance between genotypes.
C, **D**, Assessment of contrast sensitivity was with stimuli of distinct spatial frequencies that were presented at different contrast levels (1 corresponds to 100 % and 20 to ~ 5 % contrast, see icons (left)). No overt differences were observed between genotypes.

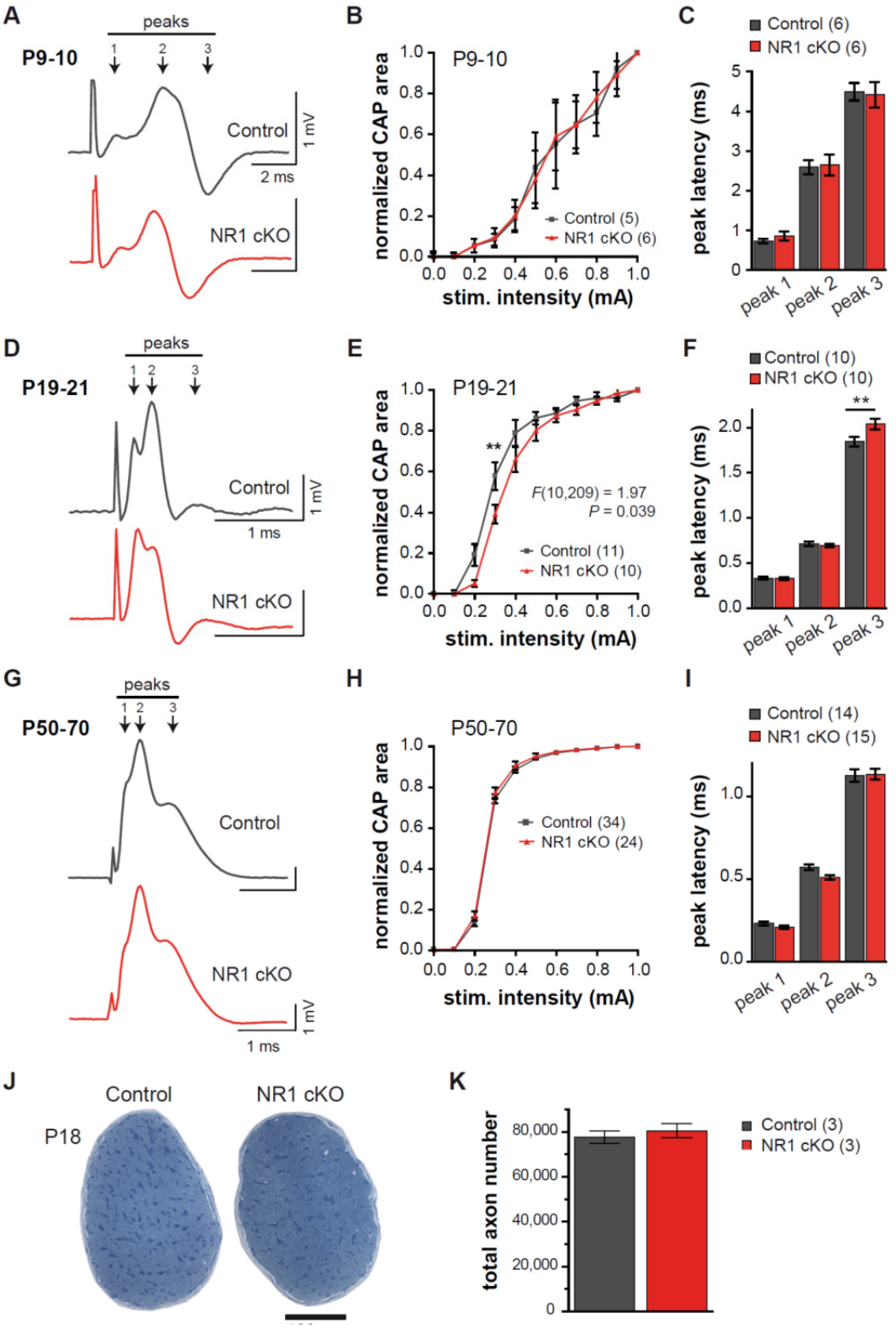

Figure S4 (Related to Figure 3). Optic nerve conduction during postnatal development.
A, **D** and **G**, Representative traces of compound action potentials (CAPs) recorded from acutely isolated optic nerves at three different ages (P9-10, P19-21, and P50-70). Nerves were stimulated with 0.8 mA every 30 s for 15 min. Traces represent CAP averages. **B**, **E** and **H**, Axon excitability of optic nerves measured at different stimulus intensities (0 – 1 mA) in 0.1 mA steps. The CAP area of each stimulus step is normalized to that of maximal stimulation (1 mA).
C, **F** and **I**, Peak latencies of averaged CAPs, recorded at the corresponding ages. **E**, At ages P19-P20, when all optic nerve axons are myelinated, mutant optic nerves displayed a reduction in axon excitability: $F_{interaction}$ (10, 209) = 1.97, P = 0.039, $F_{genotype}$ (1, 209) = 11.71, P = 0.0007, two-way Anova. At stimulus intensities up to 0.3 mA, nerves from controls responded with 58 ± 7 % and nerves from NR1 cKO with 39 ± 5 % of maximal response at 1 mA, ** P < 0.01, two-way Anova, Bonferroni post-test.

F, The conduction delay of peak 3 from NR1 mutants was significantly increased at P19-20 (1.85 ± 0.05 ms vs. 2.04 ± 0.06 ms in control and NR1 cKO, respectively, $P < 0.01$, two-way Anova, Bonferroni posttest). In contrast, in unmyelinated (a – c, P9-10) and in adult, fully myelinated optic nerves (g – i, P50-70) the conduction properties were equal between controls and NR1 mutants.
J, Semi-thin cross sections from epoxy-embedded optic nerves at P18 from control (left) and NR1 cKO (right) mice. No overt difference was observed in nerve cross section area (3 nerves per genotype analysed). Scale bar 100 µm.
K, Total axon number was not altered in NR1 cKO optic nerves (80520 ± 1875) compared to littermate controls (77680 ± 1650, n =3, $P = 0.32$ Student t test). For each optic nerve 400-760 axons from 5-8 randomly taken EM images were counted. Average axon density of each nerve was multiplied with the average total cross section area subtracted from the fraction of non-axonic (glial cell bodies and processes) area.

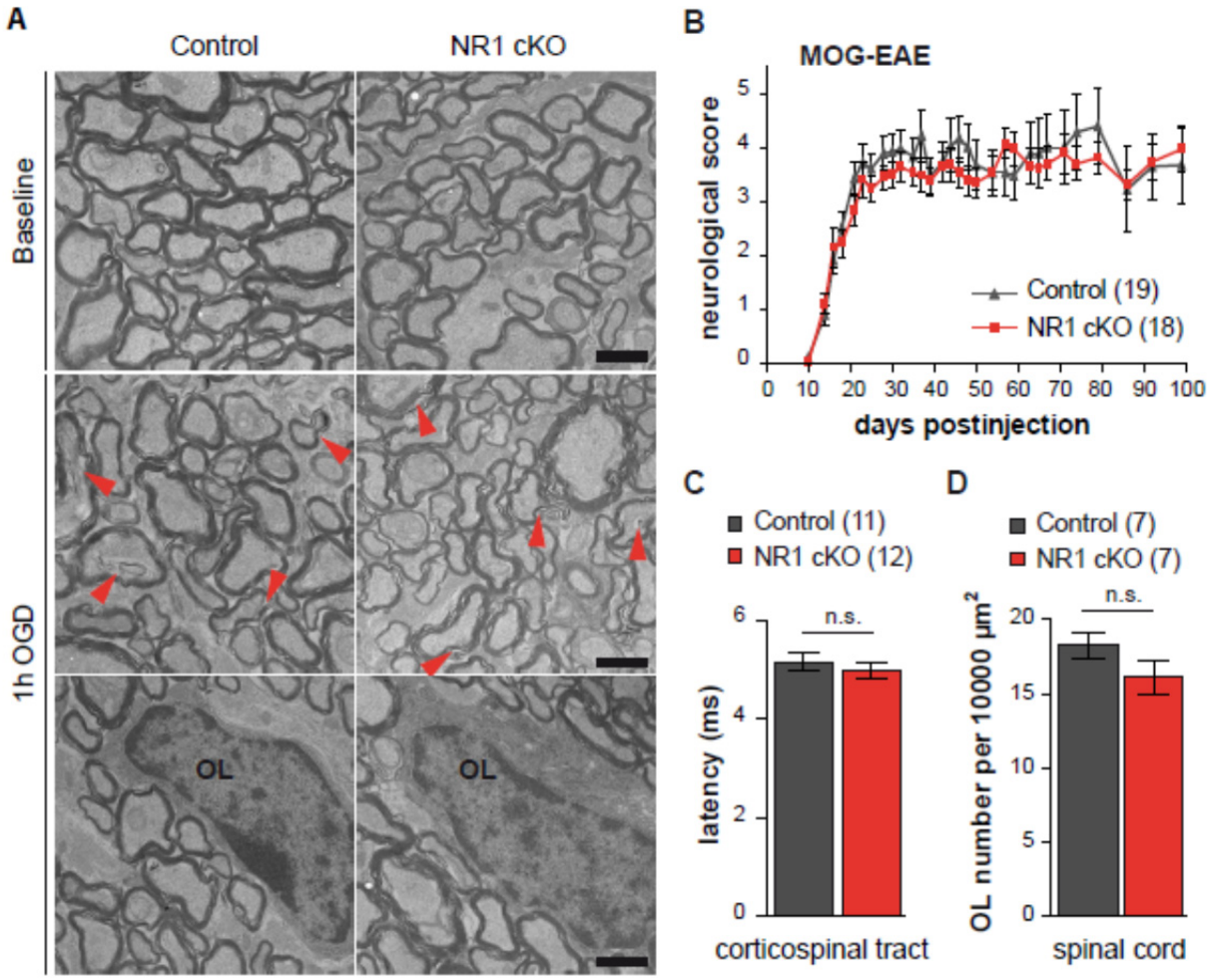

Figure S5 (Related to Figure 4). NR1 mutant white matter tracts are not more vulnerable to injury.
A, Electron microscopic inspection of optic nerves that were subjected to 1 h baseline (upper panel) and 1 h oxygen glucose deprivation (OGD) (middle and lower panel). Ultrastructural damage such as occasional loosening of the myelin sheath (red arrowheads) was identical in both controls and NR1 mutants. In both genotypes there were no morphological signs of oligodendrocyte (OL) death (lower panel). Scale bar 1 µm.
B, Time course of EAE-associated neurological symptoms. Control mice (n=19) and NR1 cKO mice (n=18) were immunized with MOG35-55 peptide and exhibited similar EAE scores, with no difference in the onset of symptoms or severity (see Methods for score).
C, The axon conduction latency in the corticospinal tract of mice with chronic EAE (measured at the end of the EAE experiment) was similar in both groups of animals (control 5.15 ± 0.17 ms (n = 11) vs NR1 cKO 4.98 ± 0.16 ms (n = 12)).
D, At the end of the EAE experiment, the density of oligodendrocytes (CC1+ cells/1,000 µm2) in the spinal cord was not different in NR1 cKO mice (control 18.3 ± 0.9 (n = 7) vs NR1 cKO 16.1 ± 1.2 (n = 7).

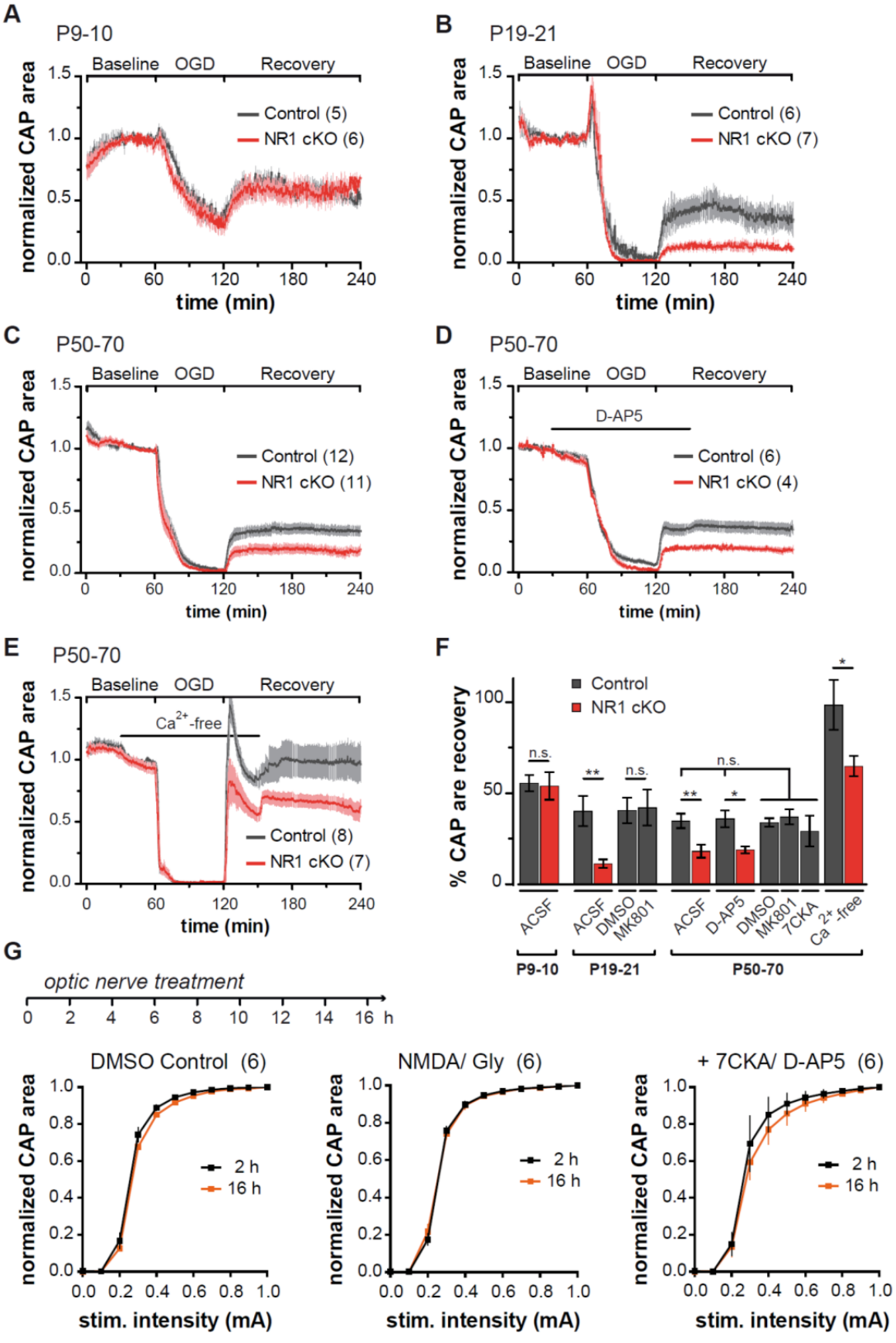

Figure S6 (Related to Figure 4). Recovery of axon function from OGD decreases with myelination and acute NMDA receptor inhibition does not mimic NR1 deficiency

A-E, After 1 h baseline recording (perfused with oxygenated ACSF) optic nerves are subjected to 60 min OGD and then reperfused for a 2 h recovery period with oxygenated ACSF. Functional integrity of axons over time was monitored by quantifying the area under the CAPs (evoked by a supramaximal stimulus) and normalizing to baseline.

A, At P9-10 (when axons are not yet fully myelinated) optic nerves from NR1 cKO showed the same functional decline following OGD and recovery thereafter.

B, At P19-21, myelinated optic nerves from control and NR1 cKO mice exhibited the same rapid loss of conduction, but after OGD nerves from NR1 mutants recovered less well.
C, Following transient OGD optic nerves from adult (fully myelinated) NR1 mutant mice recover less well (-50%) than nerves from littermate controls (same image as in Figure 4A).
D, Incubation of optic nerves from wildtype and NR1 mutants with the NMDA receptor blocker D-AP5 (50 μM, 30 min before OGD onset) did not reveal overt differences of the CAP time course and recovery from OGD when compared to control conditions (ACSF). Note that NR1 mutants recovered -50% when compared to control nerves, suggesting a largely developmental defect.
E, Optic nerves from controls and NR1 mutants were exposed to transient OGD in Ca^{2+}-free conditions (4 mM Mg^{2+} containing 200 μM EGTA). In the absence of free Ca^{2+} axonal recovery is improved in both mutants and controls. Note that axons from NR1 mutants still recovered less well.
F, Comparison of functional axon recovery under different experimental conditions. Wildtype optic nerve axons that were treated with D-AP5, 7CKA or MK801 to acutely block NMDA receptors revealed comparable recovery to nerves under control (ACSF) conditions. Similarly, NR1 mutant optic nerves had equivalent recoveries with or without D-AP5 treatment. Under Ca2+ free conditions control optic nerves recovered up to 98 ± 14 % (n = 8) whereas axons from NR1 mutants revealed a recovery of 65 ± 6 % (n = 7), $P < 0.05$ Student t test.
G, Wildtype optic nerves maintained *ex vivo* for 16 hours in oxygenated ACSF and treated with either NMDA/ Gly (100 μM), or NMDA/ Gly plus 7CKA/ D-AP5 (100 μM) or DMSO (solvent control), were tested for functional integrity and conductivity by applying increasing stimulus intensities (0 – 1 mA) in 0.1 mA steps. Depicted are stimulus-response relationships. Nerve conduction properties were tested at 2 and 16 hours of incubation for each treatment group. Note that there were no overt changes in nerve excitability over 16 hours of treatment, indicating functional integrity of optic nerves (See also Figure 4G).

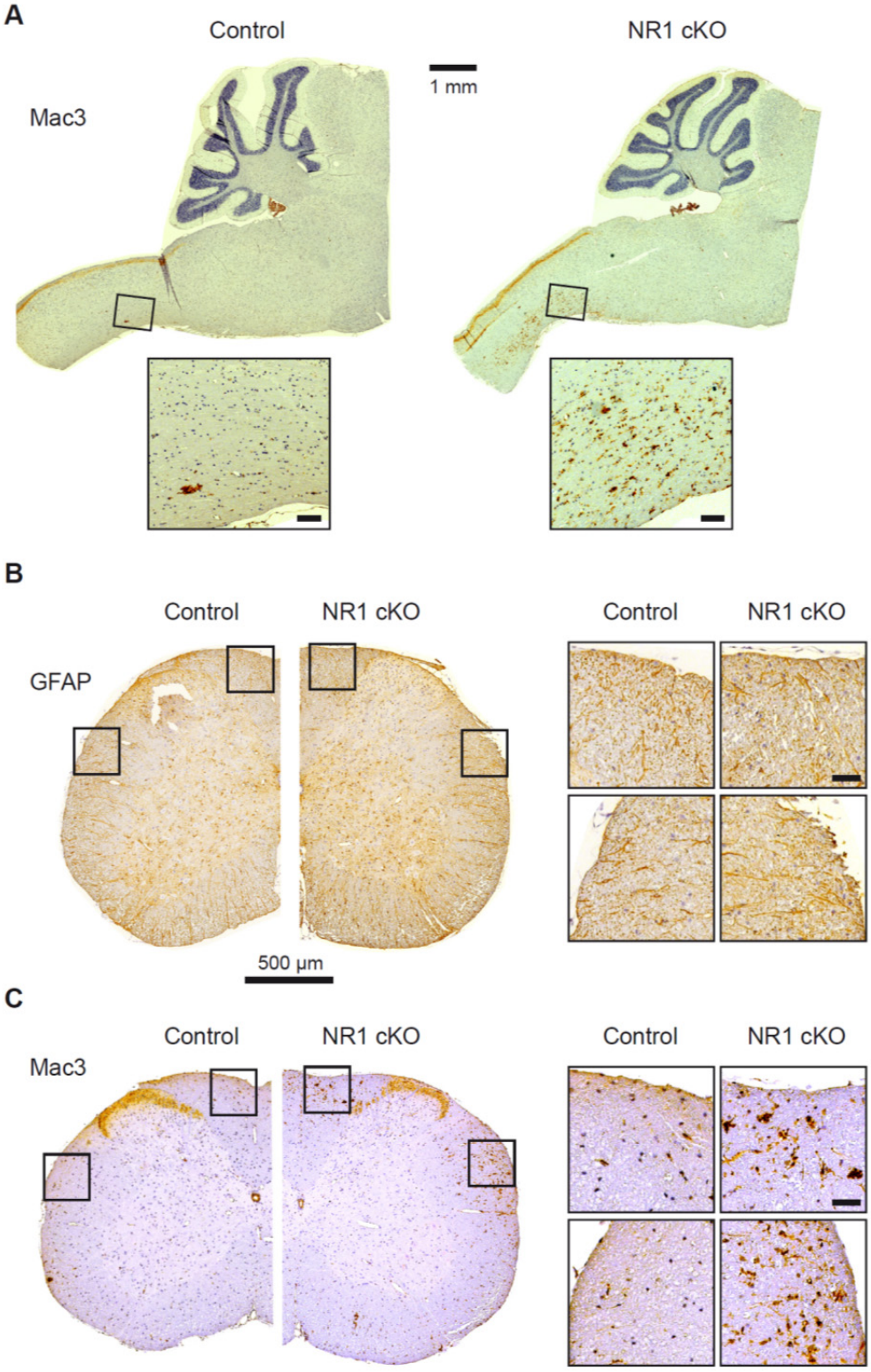

Figure S7 (Related to Figure 6). White matter tracts of brain stem and spinal cord show signs of inflammation
A, Depicted are longitudinal sections of cerebellum, brainstem and spinal cord (age 10 months), immunostained for activated microglia/macrophages (Mac3). In the ventral spinal cord, where the majority of cortico-spinal axons pass, we observed a significant increase of this inflammation marker in NR1 mutant mice (see also Figure 6).
B, **C** Spinal cord cross-sections from control and NR1 mutant mice stained (**B**) for astrogliosis (GFAP) and (**C**) for activated microglia/macrophages (Mac3).
Black boxes mark regions of higher magnifications; scale bars 100 µm (A) and 50 µm (B, C).

Supplemental Experimental Procedures

Purification of OPCs by immunopanning.

OPCs utilized for biotinylation assays, for measurements of 2-deoxyglucose uptake or lactate release by NMR were further purified to 98.2±0.3% by negative selection immunopanning (Barres et al., 1992). To selectively remove microglia, single cell suspensions of mechanically dissociated OPCs were incubated on Petri dishes coated with Bandeiraea simplicifolia (BS) lectin1(Cahoy et al., 2008) (2.3µg/ml, Vector labs) for 15 min at 37°C. To selectively remove astrocytes, unattached OPCs and astrocytes were then incubated for 30 min at 37°C on dishes sequentially coated with anti-mouse IgG antibody (Jackson Immunoresearch) and anti-rat neural antigen-2 (RAN-2) (Bartlett et al., 1981) antibody (i.e. conditioned media from RAN-2 hybridoma B lymphocytes (ATCC). The remaining purified OPCs were plated and differentiated as described in Experimental Procedures.

Glucose sensor FRET imaging

For glucose sensor confocal imaging, coverslips containing transfected primary oligodendrocytes were transferred to a custom made imaging chamber and continuously perfused with ACSF (in mM: NaCl 110.34; KCl 5.33; NaH_2PO_4 0.906; $NaHCO_3$ 44.05; $MgSO_4$ 0.814; $CaCl_2$ 1.8; glucose 10; adjusted to pH 7.4 with HCl after equilibration with 5% CO_2). The chamber was mounted on a Leica SP5 confocal microscope and cells were imaged using a HCX PL APO lambda blue 63x1.20 water-immersion objective. CFP was excited at 458 nm, and emission filters were set at 470-500 nm and 520-570 nm for detection of CFP and YFP fluorescence, respectively. Images were acquired every 10 s. Region of interests were set comprising the soma and the major processes of transfected oligodendrocytes. Background corrected mean fluorescence intensities were corrected for spectral bleed-through using correction factors obtained by transfecting primary oligodendrocytes with CFP or YFP only (Hou et al., 2011). Finally, corrected YFP fluorescence intensity obtained after excitation of CFP (= FRET) was divided by the corrected CFP fluorescence and the ratio (Fc/CFP) was normalized to the first 5 min of baseline recording, which was set as 1. NMDARs were activated by changing the perfusion solution to ACSF containing 100 µM NMDA and 100 µM glycine. Cells were preincubated with the antagonists of NMDA receptors (7CKA, 100 µM; D-AP5, 100 µM) for 30 min before NMDA and glycine were applied. For control experiments cells were incubated in ACSF lacking glucose or containing either iodoacetate (inhibitor of glycolysis, 1 mM) or cytochalasin B (inhibitor of glucose transpoter, 40 µM). From these data, the Fc/CFP signal was calibrated to cytosolic glucose concentrations using the k_D = 700 µM of the glucose sensor for glucose as described (Bittner et al., 2010). We have continuously monitored the cellular morphology of transfected oligodendrocytes by concomitant time lapse imaging to determine that drug applications (e.g. cytochalasin B) did not cause morphological changes that influence FRET signals.

NMR analysis

Conditioned media from untreated and 30 min NMDA/Gly (100 µM) treated immunopanned oligodendrocytes were snap frozen. Samples were mixed with 10% D_2O and the internal standard DSS and transferred to 3 mm NMR tubes. All spectra were recorded on an Avance Bruker 700 MHz spectrometer equipped with a cryogenic TXI $^{1}H/^{13}C$-$^{15}N/^{2}H$ probe head at 4°C. The ^{13}C, ^{1}H-HSQC experiments were done by acquisition of 2048 points in the direct dimension with spectral width of 13 ppm and 300 increments in the indirect dimension with spectral width of 95 ppm. The *J* coupling defocusing delay was set to 4 ms ($1/2^{1}J_{HC}$), the recycling time to 1.2 s and the total acquisition time was 3 hours and 46 minutes for each sample. A polynomial baseline correction was applied to the time domain signal. The latter was then zero filled to 4096 and 1024 points in the direct and indirect dimensions, respectively. Afterwards the time domain data were apodized by multiplication with a cosine function set to 0 at t_{1max} and Fourier transformed to the frequency domain in both dimensions. The data processing was performed using nmrPipe software (Delaglio et al., 1995). The integrations and quantifications were done using CARA (Keller, 2004).

Lactate release by fluorometric measurement of NADH

Lactate release from cultured oligodendrocytes was analysed as described for astrocytic cultures (Requardt et al., 2010). Mouse oligodendrocyte precursor cells were prepared as described above, 50,000 cells were seeded in wells of 24-well cell culture plates and were allowed to differentiate for 5 days in SATO medium. Cells were washed once with ACSF containing 10 mM glucose, and preincubated in 250 µl of ACSF (control) or ACSF containing 100 µM 7-CKA and/or 100 µM D-AP5 for 30 min. Then, cells were incubated in 250 µl ACSF with or without 100 µM NMDA and 100 µM glycine in the presence or absence of the inhibitors. For inhibition of glucose transporters, cytochalasin B was added in the concentrations indicated in the figures. After 15, 30 and 60 min of incubation 20 µl medium was removed and lactate content was determined using a reaction mixture consisting of 0.5 M glutamate buffer pH 8.9, 6 mM NAD^+, 35 µg/ml glutamate pyruvate transaminase and 50 µg/ml lactate dehydrogenase. After 60 min at 37 °C NADH fluorescence was determined using a plate reader and compared to wells containing known concentrations of lactate. Protein determination was done according to the Lowry method using bovine serum albumin as a standard.

Immunohistochemistry

Mice were anesthetized (2,2,2-tribromoethanol (2 % v/v) and amyl alcohol (2 % w/v, 0.2 ml/ 10 g body weight) and subsequently perfused with 4% paraformaldehyde (PFA) in 0.1 M sodium phosphate buffer. Brains and optic nerves were isolated and kept in the same fixative for 8-12 h at 4°C. After washing with PBS, optic nerves were cryoprotected with sucrose and frozen in OCT compound (Shandon Cryomatrix, Thermo Scientific) on dry ice. Nerve sections of 12 µm were made on a cryostat (Leica, Jung 2045C), mounted on superfrost slides (Superfrost Plus, Thermo Scientific) and air dried at room temperature (RT). Slide-mounted sections were washed with PBS and treated with 0.3% Triton X-100 and 5% horse serum for 1 h at RT. Brain sections of 40 µm were cut coronally with a vibratome (Leica, VT1000S) and treated similarly.

Primary antibodies were incubated over night at 4°C in 0.3% Triton X-100 and 5% horse serum. Dilutions were as follows: GFP (1:800, goat, Rockland; 1:500, rabbit, Abcam), CC1 (1:50, mouse, Calbiochem), Olig2 (1:200, rabbit, gift from C. D. Stiles, Boston, MA, USA), NG2 (1:200, rat, gift from J. Trotter, Mainz, Germany), GFAP (1:100, mouse, Novocastra), IBA1 (1:100, rabbit, Wako), NR1 (1:250, mouse, Zymed Laboratories), MBP (1:300, rabbit, Dako).

Secondary antibodies to mouse, rabbit and goat conjugated to Alexa 488-(1:2000 Molecular Probes), Alexa-555-(1:2000, Molecular Probes), Alexa-633(1:500, Molecular Probes), Cy2-(1:100, Dianova), Cy3-(1:1000, Dianova) and Cy5-(1:500, Dianova) were incubated in 2 % horse serum for 2 h at RT. For nuclei labeling DAPI (0.025 µg/ml final concentration) was added to the secondary antibody.

Confocal images were collected with a LSM 510 Meta microscope (Zeiss) using a 20x/0.5 Plan-Neofluar and 40x/1.2 water-immersion C-Apochromat objective. Excitation was performed at 488 nm, 543 nm and 633 nm, emission was detected for Alexa 488/Cy2, Alexa 555/Cy3 and Alexa 633/Cy5 at 500-530 nm band-pass, 560 nm long-pass and 650-710 nm band-pass filter sets, respectively. Z-stack images were taken at 0.5 – 1 µm intervals. For reporter analysis confocal stacks of 2-3 different sections from 3-4 individual animals were analyzed. For quantification of relative NR1 fluorescence intensities 9-12 confocal stacks of 3-4 different longitudinal optic nerve sections of 3 individual animals for each genotype were analyzed. The average fluorescence intensity for all stacks was calculated using ImageJ. Data were grouped per animal and normalized to controls.

Assessment of genomic recombination

Real time quantitative PCR (using SYBR Green and a 7500 Fast Real-Time PCR System, Applied Biosystems) was performed to amplify a DNA sequence of 184 bp flanking the 5' loxP site within the 5 kb intron between exons 10 and 11 of the floxed NR1 locus. Primers were located closely up- and downstream of the 5' loxP site and had the following sequence: sense 5'-GTCAAGCTTAGGATCCGGAACC-3' and anti-sense 5'-CAACTGCTCTTCCGAAGGTC-3'. Only non-recombined alleles would be amplified whereas after successful recombination the anti-sense primer could not anneal to its complementary strand impeding the PCR amplification. Genomic DNA was isolated from optic nerves of individual animals. For each sample four technical replicates per PCR were implemented. Neuregulin 1 type III (NrgIII) (sense 5'-GTGTGCGGAGA-AGGAGAAAACT-3' and anti-sense 5'-AGGCACAGAGAGGAATTCATTTCTTA-3') and Gria1 (sense 5'-CCAGGTGTCTT-CTCCTTTCTTG-3' and anti-sense 5'-CTGAAACGGCTGACCAGG-3') were used as endogenous gene controls. Data normalization and analysis were performed with the 7500 Fast System Software. This approach enabled a relative quantification of the extent of recombined alleles in the optic nerves of NR1 cKO mice.

Electron microscopy

Following tissue preparation and fixation, samples were dehydrated in a graded series of ethanol, and then embedded in Epon. For HPF freshly dissected optic nerves were placed in an aluminum specimen carrier with a 0.1 mm or 0.2 mm indentation (Microscopy Services, Kiel, Germany). Remaining space was covered with yeast paste or 20% PVP in PBS, and the sample was cryofixed in a Bal-Tec HPM010 high-pressure freezer (former Bal-Tec, now ABRA-Fluid AG, Widnau, Switzerland). Freeze-substitution was carried out in a Leica AFS (Leica, Vienna, Austria) as follows: Samples were first kept in tannic acid (Sigma-Aldrich) 0.1% in acetone at −90°C for 100 h, washed with acetone (4 x 30 min, −90°C), and then transferred into OsO_4 (Science Services, Munich, Germany) 2 % in acetone, −90°C. The temperature was raised from −90°C to −20°C in increments of 5°C/h, then kept unaltered at −20°C for 16 h, and then raised from −20°C to +4°C in increments of 10°C/h. Then the samples were washed with acetone (3 x 60 min at 4°C), allowed to adjust to room temperature (1 h), and finally transferred into Epon (Serva) (50% Epon in acetone for 3 h, 90% Epon in acetone for 18 h, 100% Epon for 6 h). The samples were placed in an embedding mold and polymerized (60°C, 24 h). Ultrathin sections (50 nm) were cut using a Leica Ultracut S ultramicrotome (Leica, Vienna, Austria) and stained with an aqueous solution of 2% uranyl acetate (Merck, Darmstadt, Germany) followed by lead citrate (Reynolds, 1963).

Optic nerve recordings analysis

Acutely isolated optic nerves were stimulated and recorded from by custom-made suction electrodes back-filled with ACSF [(in mM): 124 NaCl, 3.0 KCl, 2.0 $CaCl_2$, 2.0 $MgSO_4$, 1.25 NaH_2PO_4, 23 $NaHCO_3$, and 10 glucose]. The stimulation electrode was connected to a stimulus isolator (385, WPI) to evoke compound action potentials (CAP). The recording electrode was connected to a Heka amplifier (EPC9), and the signal was amplified 500 times, filtered at 30 kHz, and acquired at 20-30 kHz. Before recording, optic nerves were equilibrated for at least 15 min in the chamber. Square-wave constant current stimulus

pulse (50 µs) strength was adjusted to evoke the maximum CAP possible, and then increased an additional 25 % for supramaximal stimulation.

Stimulus-response relationships were performed by varying stimulus intensity from 0.1 to 1 mA and measuring the area of the corresponding graded CAPs. This protocol allowed for comparison of the relative thresholds of activation of the population of conducting fibers. The CAP area was expressed as percentage of the last CAP area (at maximum stimulation of 1 mA) in the train.

The CAP latency was measured (at supramaximal stimulation after averaging 50 CAPs elicited every 30 s) as the time between the onset of the stimulus artefact to the first, second and third peak as previously described (Baltan et al., 2010). The suction electrode recording configuration at supramaximal stimulation allows all axons in optic nerves to be activated and the resultant action potential from each axon to be recorded. This method has the advantage of enabling stable recording of three-peaked characteristic shape of CAPs. These peaks reflect three sub-groups of axon populations based on their conduction velocity and the area under the CAP reflecting the number of contributing axons (Cummins et al., 1979).

For pharmacology of OGD recordings the following experiments were performed. A Ca^{2+}-free ACSF was used in some experiments and contained 200 µM EGTA and 4 mM Mg^{2+} (to maintain constant divalent cation concentration). Control experiments indicated that CAPs remained essentially unchanged in this solution (with normal glucose and oxygen) for at least 90 min. 7-chlorokynurenic acid (7-CKA, 50 µM; dissolved in DMSO as 50 mM stock), D-(-)-2-Amino-5-phosphonopentanoic acid (D-AP5, 100 µM) and MK801 (50 µM, dissolved in DMSO as 50 mM stock) were used to block NMDA receptors during recordings. Optic nerves treated with pharmacological substances or Ca^{2+}-free ACSF were incubated 30 min before, during and 30 min after OGD.

Surgery for in vivo spinal cord CAP recordings

Surgery for in vivo spinal cord recordings was slightly modified as previously described (Dibaj et al., 2012; Steffens et al., 2012). Anaesthesia was initiated by 80 mg/kg pentobarbital injected i. p. After cannulation of the jugular vein, anesthesia was continued with 40-60 mg methohexital per kg and h. A tracheotomy was performed and a tube inserted for artificial ventilation. Active respiratory movements were abolished by paralysis with pancuronium (800 µg per kg supplemented i.p. every hour) and artificial ventilation with a gas mixture of CO_2 (2.5 %), O_2 (47.5 %), and N_2 (50 %) at 120 strokes/min (100-160 µl/stroke depending on the body weight) was performed. Body temperature, heart rate and O_2 blood saturation were continuously monitored and also used to control the level of anesthesia. The vertebral column was rigidly fixed with two custom-made clamps. A laminectomy was performed from vertebrae TH13 to L5 to expose the spinal cord segments L1 to L4 as well as to expose the dorsal roots L3 to L5. For electrophysiology, the spinal cord was covered with mineral oil.

Behavioural assessment of visual acuity and contrast sensitivity

Visual acuity and contrast sensitivity response were assessed using the virtual-reality optomotor system (Douglas et al., 2005; Prusky et al., 2004). In the optomotor system freely moving animals were exposed to moving sine wave gratings of various spatial frequencies, contrasts and drift speeds and reflexively tracked this pattern by head movements as long as they could see it. Experimenters were blind to the animal's genotype and thresholds were regularly validated independently by more than one observer.

Experimental autoimmune encephalomyelitis (EAE) induction

EAE experiments were carried out in 8-12 week-old mice as described earlier (Matute et al., 2007). Briefly, chronic, relapsing EAE was induced in littermate control and in NR1 cKO mice, by immunization with 300 µl of myelin oligodendrocytes glycoprotein 35–55 [MOG(35–55)] (200 µg; Sigma) in incomplete Freund's adjuvant supplemented with 8 mg/ml *Mycobacterium tuberculosis* H37Ra. Pertussis toxin (500 ng; Sigma) was injected intraperitoneally on the day of immunization and again 2 d later. In all instances, motor symptoms were recorded daily and scored as follows from 0 to 8: 0, no detectable changes in muscle tone and motor behaviour; 1, flaccid tail; 2, paralyzed tail; 3, impairment or loss of muscle tone in hind limbs; 4, hind limb hemi-paralysis; 5, complete hind limb paralysis; 6, complete hind limb paralysis and loss of muscle tone in forelimbs; 7, tetraplegia; and 8, moribund. Conduction velocity of the corticospinal tract was assessed in anesthetized mice with tribromoethanol (240 mg/kg, i.p.; Sigma) using stimulatory and recording electrodes placed in the primary motor cortex and in the vertebral canal at the L2 level, respectively. After recording, mice were fixed, and spinal cord was processed for immunohistochemistry. Tissue blocks of spinal cords were cryoprotected, cut longitudinally (10 µm thick), and stained with toluidine blue and antibody to CC1 (1 µg/ml; Calbiochem, Barcelona, Spain).

Supplemental References

Baltan, S., Inman, D.M., Danilov, C.A., Morrison, R.S., Calkins, D.J., and Horner, P.J. (2010). Metabolic vulnerability disposes retinal ganglion cell axons to dysfunction in a model of glaucomatous degeneration. JNeurosci *30*, 5644-5652.

Barres, B.A., Hart, I.K., Coles, H.S., Burne, J.F., Voyvodic, J.T., Richardson, W.D., and Raff, M.C. (1992). Cell death and control of cell survival in the oligodendrocyte lineage. Cell *70*, 31-46.

Bartlett, P.F., Noble, M.D., Pruss, R.M., Raff, M.C., Rattray, S., and Williams, C.A. (1981). Rat neural antigen-2 (RAN-2): a cell surface antigen on astrocytes, ependymal cells, Muller cells and lepto-meninges defined by a monoclonal antibody. Brain research *204*, 339-351.

Bittner, C.X., Loaiza, A., Ruminot, I., Larenas, V., Sotelo-Hitschfeld, T., Gutierrez, R., Cordova, A., Valdebenito, R., Frommer, W.B., and Barros, L.F. (2010). High resolution measurement of the glycolytic rate. Frontiers in neuroenergetics *2*.

Cahoy, J.D., Emery, B., Kaushal, A., Foo, L.C., Zamanian, J.L., Christopherson, K.S., Xing, Y., Lubischer, J.L., Krieg, P.A., Krupenko, S.A.*, et al.* (2008). A transcriptome database for astrocytes, neurons, and oligodendrocytes: a new resource for understanding brain development and function. JNeurosci *28*, 264-278.

Cummins, K.L., Dorfman, L.J., and Perkel, D.H. (1979). Nerve fiber conduction-velocity distributions. II. Estimation based on two compound action potentials. ElectroencephalogrClinNeurophysiol *46*, 647-658.

Delaglio, F., Grzesiek, S., Vuister, G.W., Zhu, G., Pfeifer, J., and Bax, A. (1995). NMRPipe: a multidimensional spectral processing system based on UNIX pipes. Journal of biomolecular NMR *6*, 277-293.

Dibaj, P., Zschuntzsch, J., Steffens, H., Scheffel, J., Goricke, B., Weishaupt, J.H., Le Meur, K., Kirchhoff, F., Hanisch, U.K., Schomburg, E.D.*, et al.* (2012). Influence of methylene blue on microglia-induced inflammation and motor neuron degeneration in the SOD1(G93A) model for ALS. PloS one *7*, e43963.

Douglas, R.M., Alam, N.M., Silver, B.D., McGill, T.J., Tschetter, W.W., and Prusky, G.T. (2005). Independent visual threshold measurements in the two eyes of freely moving rats and mice using a virtual-reality optokinetic system. VisNeurosci *22*, 677-684.

Hou, B.H., Takanaga, H., Grossmann, G., Chen, L.Q., Qu, X.Q., Jones, A.M., Lalonde, S., Schweissgut, O., Wiechert, W., and Frommer, W.B. (2011). Optical sensors for monitoring dynamic changes of intracellular metabolite levels in mammalian cells. NatProtoc *6*, 1818-1833.

Keller, R. (2004). Computer Aided Resonance Assignment. http://cara.nmr.ch.

Matute, C., Torre, I., Perez-Cerda, F., Perez-Samartin, A., Alberdi, E., Etxebarria, E., Arranz, A.M., Ravid, R., Rodriguez-Antiguedad, A., Sanchez-Gomez, M.*, et al.* (2007). P2X(7) receptor blockade prevents ATP excitotoxicity in oligodendrocytes and ameliorates experimental autoimmune encephalomyelitis. JNeurosci *27*, 9525-9533.

Prusky, G.T., Alam, N.M., Beekman, S., and Douglas, R.M. (2004). Rapid quantification of adult and developing mouse spatial vision using a virtual optomotor system. Invest OphthalmolVisSci *45*, 4611-4616.

Requardt, R.P., Wilhelm, F., Rillich, J., Winkler, U., and Hirrlinger, J. (2010). The biphasic NAD(P)H fluorescence response of astrocytes to dopamine reflects the metabolic actions of oxidative phosphorylation and glycolysis. Journal of neurochemistry *115*, 483-492.

Reynolds, E.S. (1963). The use of lead citrate at high pH as an electron-opaque stain in electron microscopy. JCell Biol *17*, 208-212.

Steffens, H., Dibaj, P., and Schomburg, E.D. (2012). In vivo measurement of conduction velocities in afferent and efferent nerve fibre groups in mice. Physiol Res *61*, 203-214.